# Enhanced performance of molecular electrocatalysts for $CO_2$ reduction in a flow cell following $K^+$ addition

Shunsuke Sato[1]*, Keita Sekizawa[1], Soichi Shirai[1], Naonari Sakamoto[1], Takeshi Morikawa[1]

**Affiliations:**

[1]Toyota Central Research and Development Laboratories, Incorporated, Nagakute, Aichi 480-1192, Japan.

* To whom correspondence should be addressed. E-mail:ssato@mosk.tytlabs.co.jp

**Abstract:** Electrocatalytic $CO_2$ reduction is a key aspect of artificial photosynthesis systems designed to produce fuels. Some molecular complexes can act as electrocatalysts for $CO_2$ reduction and the performance of these compounds can be controlled by varying their ligands and substituents. However, these compounds also suffer from poor durability and energy conversion efficiency. The present work demonstrates the drastically improved $CO_2$ reduction activity exhibited by molecular catalysts in a membrane electrode assembly cell. These catalysts were composed of a cobalt-tetrapyridino-porphyrazine complex supported on carbon black together with a potassium salt, and were both stable and efficient. These systems were found to promote electrocatalytic $CO_2$ reduction with a current density of 100 mA/cm$^2$ and generated CO over a span of at least one week with a selectivity of approximately 95%. The optimal catalyst gave a turnover number of 3,800,000 and an energy conversion efficiency more than 62% even at 200 mA/cm$^2$.

**Main Text:** The development of photocatalytic systems capable of synthesizing useful organic compounds by reducing carbon dioxide ($CO_2$) under sunlight is an increasingly important research area that addresses both global warming and fossil fuel shortages. However, the direct solar-powered reduction of $CO_2$ to organic chemicals utilizing electrons and protons extracted from water, mimicking photosynthesis in plants, is much more difficult than $H_2$ generation via water splitting. Recently, solar-driven $CO_2$ reduction with over 10% solar conversion efficiency was reported, using a solar cell incorporating electrocatalysts such as Ag metal (*1, 2*). The high solar conversion efficiency of this device can be partly attributed to the superior electrocatalytic activity of the Ag catalyst. This result indicates that the development of electrocatalytic $CO_2$ reduction catalysts will play a key role in realizing artificial photosynthesis systems.

Electrocatalytic $CO_2$ reduction can be conducted using metal or molecular catalysts (that is, metal complexes) under specific electrical bias conditions. These materials require the application of a large electrical potential to achieve catalytic $CO_2$ reduction because the first step in $CO_2$ conversion is the formation of a $CO_2^{•-}$ radical anion intermediate during single-electron reduction (*3*). The electrocatalysts that are currently used are able to facilitate proton-coupled multi-electron reactions (for example, $CO_2 + 2H^+ + 2e^- \rightarrow CO + H_2O$, -0.11 V *vs*. RHE) that require lower potentials than single-electron reactions (*4*). However, many $CO_2$ reduction catalysts have deficiencies such as low product selectivity in the presence of water due to the

preferential formation of $H_2$ at 0.0 V (*vs*. RHE). In contrast, metals such as Au and Ag can act as electrocatalysts for selective $CO_2$ reduction in $NaHCO_3$ solutions but the associated overpotentials are high (greater than 600 mV) (*5*). The market prices of certain hydrocarbon products (including CO, MeOH and $C_2H_4$) are significantly lower than those of other fine chemicals (*6, 7*). Therefore, the development of a carbon neutral society based partly on electrocatalytic $CO_2$ reduction will require the development of systems operating at low overpotentials (that is, low cell voltages) while exhibiting increased current densities, good selectivity and significant durability. Recently, the current densities associated with $CO_2$ reduction have been drastically increased through the use of gas diffusion layer electrolyzers (*8-12*). Values in excess of several hundred $mA/cm^2$ have been reported based on incorporating metal catalysts such as Au, Ag and Cu. Despite this, $CO_2$ reduction catalysts still require improvement in several areas. As an example, because of the low mass-based catalytic activity during $CO_2$ reduction provided by present day materials, relatively large masses of noble metals must be used. In addition, the electrical-to-chemical conversion efficiencies obtainable during $CO_2$ reduction in conjunction with water oxidation (meaning the energy conversion efficiency) are presently insufficient even when using noble metals (see Table S1). One of the reviews have reported that the energy conversion efficiency of electrocatalytic $CO_2$ conversion must be greater than 60% at a current density of several hundred $mA/cm^2$ to allow this process to become competitive with fossil fuel prices (*6*). However, the energy conversion efficiency of $CO_2$ electrolysis at room temperature was typically less than 40% over long-term experiments (*13*). The cost of electrolyzers is also an important aspect of the economic viability of this process, and so there is a need for new, non-noble catalysts for $CO_2$ reduction that meet the criteria described above.

A number of molecular catalysts have also been used in gas diffusion layer electrolyzers(*14-18*). Although these compounds have exhibited high current density values during $CO_2$ reduction, there are associated deficits, such as low durability and poor energy conversion efficiencies (meaning high cell voltages or overpotentials). The poor durability of these materials is especially concerning (*19*). As an example, it has been reported that a cobalt phthalocyanine (Co(Pc)) catalyst with phenol as an additive produced a good current density of 150 $mA/cm^2$ during $CO_2$ reduction at approximately -2.3 V in   a zero-gap membrane electrode assembly (MEA) cell. Although this device was able to promote the $CO_2$ reduction reaction without resistance compensation, the catalytic activity of the Co(Pc) was maintained for less than several hours (at which point the current density decreased below 100 $mA/cm^2$) and a high cell voltage was required (*14*). The $CO_2$ reduction potentials and catalytic activities of molecular catalysts can be adjusted by changing the ligands and substituents in the complex (*19*), and so it may be possible to develop new materials based on tuning the molecular design and reaction environment (*20*). The goal of such work would be to achieve the required high energy conversion efficiency along with suitable levels of current density and sufficient durability(*6, 7*).

The present work demonstrates electrocatalytic $CO_2$ reduction using a MEA cell including a cathode comprising cobalt-tetrapyridino-porphyrazine (Co(PyPc)) with potassium triflate (KOtf) as an additive on a carbon-based support, together with nickel foam incorporating iron and nickel oxide catalysts as the anode and an anion exchange membrane (AEM). The Co(PyPc) molecular catalyst showed good electrocatalytic activity during CO production from $CO_2$ in the MEA cell at a lower cell voltage than was required when using Co(Pc), because the lowest unoccupied molecular orbital (LUMO) potential of the former compound was lower than that of the latter. The electrocatalytic activity of Co(PyPc) was also drastically improved by adding $K^+$ cations to

the carbon substrate. This work therefore developed an electrocatalytic $CO_2$ conversion system capable of producing CO from $CO_2$ with high selectivity (approximately 95%) together with a low cell voltage (approximately -1.9 V), suitable energy conversion efficiency (approximately 68%) and significant durability (over one week under 100 mA/cm$^2$) with a turnover number (TON) on the order of 3,800,000.

These Co-based molecular catalysts were synthesized according to a previously reported method (21) and had the molecular structures shown in Figures 1A and B. Figures 1C and D present cyclic voltammetry (CV) data obtained from Co(PyPc) and Co(Pc) in a dimethyl formamide (DMF) solution under Ar or $CO_2$ atmospheres. The LUMO potential of Co(PyPc) was found to be lower than that of Co(Pc) by approximately 200 mV, and the former material generated a catalytic current under $CO_2$. Density functional theory (DFT) calculations also indicated that Co(PyPc) catalysts should exhibit lower LUMO potentials than Co(Pc) (22). These results demonstrate that $CO_2$ reduction using an MEA cell should proceed at a lower voltage when using Co(PyPc) instead of Co(Pc). In general, the $CO_2$ reduction activity of a molecular catalyst having a lower LUMO potential is decreased because the compound does not readily react with $CO_2$ (17, 20, 23). For this reason, the majority of research in this field has not examined molecular catalysts having lower LUMO potentials. However, the present work confirms that the synergistic effect of a carbon support and K$^+$ cations improves the $CO_2$ reduction activity of molecular catalysts with lower LUMO potentials (20). Therefore, it is possible that the electrocatalytic activity of $CO_2$ reduction using Co complex catalysts can be improved by adding K$^+$ cations in a MEA cell, because $CO_2$ gas only is provided near the catalysts in a MEA cell, that is, there is almost no K$^+$ cation near the catalyst.

The present MEA cell consisted of a cathode, anode, AEM and a cell plate with a flow system and Teflon spacer (Figure S1). Co(PyPc) supported on carbon powder, KOtf and Nafion were drop-cast onto AvCarb gas diffusion paper to fabricate the cathode (referred to herein as Co(PyPc)+K/C). Transmission electron microscopy (TEM) images of the Co(PyPc) on carbon powder are presented in Figure S2. A Ni-doped β-FeOOH catalyst (24, 25) on a Ni foam (Ni+Fe/Ni) was used as the anode. The catalytic areas of the cathode and anode were each 1.13 cm$^2$. Wet $CO_2$ was fed to the cathode at 100 standard cubic centimeters per minute (SCCM) while a recirculated 1 M KOH solution was fed to the anode at a flow rate of 100 ml/min. The cell was equipped with an autosampler for *in situ* measurements and was directly connected to a gas chromatograph to allow the analysis of CO and $H_2$ generated as reaction products. The electrocatalytic $CO_2$ reduction trials in this cell were performed under constant current conditions over a time span of 2 h, with the results shown in Table 1. The electrocatalytic activity during CO production throughout this 2 h period, as indicated by current density, was found to be in the range of 10 to 200 mA/cm$^2$. It should be noted that, in trials without the Co(PyPc) catalyst, only $H_2$ production was observed (Figure S3).

The highest energy conversion efficiency obtained from this device was approximately 76.4% at -1.59 V. Figure 2 summarizes the efficiencies observed during CO production trials using other catalysts for $CO_2$ reduction with water oxidation at a current density 100 mA/cm$^2$. A cell voltage of approximately -1.89 V was obtained from an MEA cell containing the Co(PyPc)+K/C cathode (loaded with Co(PyPc) at 0.06 mg/cm$^2$) with the Ni+Fe/Ni anode in conjunction with a current density of -100 mA/cm$^2$ and a Faradaic efficiency of 98.2 ± 1.0% during CO production (FE(CO)) and 69.5% energy conversion efficiency. This MEA system, which uses only Earth-abundant elements such as Co, Fe and Ni, exhibits superior performance (including a low cell

voltage, high energy conversion efficiency and good mass-based activity) compared with Au and IrOx catalysts in MEA systems (for example, -100 mA/cm$^2$ at -2.0 V using Au and IrOx) ($9$). In addition, the cell voltage during $CO_2$ reduction could be lowered from -1.89 to -1.82 V by increasing the Co(PyPc) catalyst loading from 0.06 to 0.24 mg/cm$^2$. This change also provided an energy conversion efficiency of 71.2% at 100 mA/cm$^2$. These results indicated that an enhanced current density together with significant energy conversion efficiency could be obtained simply by increasing of Co(PyPc) in the device. The mass-based activity of the Co(PyPc)+K/C electrode was found to be approximately 2300 at a -2.04 V cell voltage, and so was on the order of five times greater than that reported for a Au catalyst at the same cell voltage (Figure 2B). The mass-based activity of the present catalytic system was also approximately 130 times higher than that of the Co(Pc) catalyst used in prior research at the same cell voltage ($14$). To the best of our knowledge, this catalyst exhibited the highest mass-based activity during $CO_2$ reduction, together with over 60% energy conversion efficiency using KOH solution (Table S1).

Figure 3A summarizes the electrocatalytic formation of CO over the Co(PyPc)+K/C using the MEA cell during a prolonged trial in which a reaction current of -100 mA/cm$^2$ was obtained with cell voltages (Figure 3B). The main product from this reaction was CO with an FE(CO) value of $95.0 \pm 1.4\%$ and the cell was able to demonstrate electrocatalytic activity for at least seven days (Figures 3A and B) while generating approximately 0.34 mol of CO. Considering that approximately 78 nmol of Co(PyPc) was loaded on the AvCarb substrate, the turnover frequency (TOF) for CO production was approximately 6.4 s$^{-1}$ while the TON was 3,859,745. In the case of the previous Co(Pc) catalyst, the TON was on the order of 4000 with a TOF of approximately 0.06 s$^{-1}$ using an MEA cell at a current density of 100 mA/cm$^2$. Our result showed that the improvement of TON for $CO_2$ reduction was affected by K$^+$ cations, which will be discussed later.

Although the cell voltage required for a current density of -100 mA/cm$^2$ increased during the progression of the electrolysis, the original value could be almost fully recovered by refreshing the KOH solution (Figure 3B). This effect occurred because the pH of the KOH solution decreased slightly from the initial value of 14.0 during the 24 h electrolysis ($15$). The average cell voltage at 168 h was approximately -1.95 V and the energy conversion efficiency at this point was approximately 68%. The structure of the Co(PyPc) was assessed after seven days of the reaction using X-ray photoelectron spectroscopy (XPS; Figure S4). These analyses indicated minimal change in the material after 168 h of electrolysis. Based on this structural stability and the apparent recovery of the cell voltage after replacing the KOH solution, it is apparent that the present Co(PyPc)/C+K electrode would be expected to continuously generate CO over a period of seven days. In general, MEA cells tend to suffer from the precipitation of carbonate salts at the cathode as a result of anolyte crossover ($26, 27$). Therefore, it was anticipated that the addition of the KOtf salt to the catalytic layer on the cathode would lead to precipitation in the present system. However, salt precipitation was not observed in the flow channel after seven days of electrolysis at a current density of -100 mA/cm$^2$, nor after 120 h at 150 mA/cm$^2$ (Figure S5). Even so, as expected, the flow of gaseous $CO_2$ was stopped by salt precipitation within several hours at -200 mA/cm$^2$ (Figure S6). These results are in agreement with prior work ($27$) showing that salt precipitation is greatly affected by the amount of anolyte crossover and that K$^+$ cations from this process are almost always consumed by salt precipitation. Based on these results and previous reports, we believe that the salt precipitation in the flow channel is not due to the presence of K$^+$ cations, but can be primarily attributed to OH$^-$ anions resulting from anolyte crossover. Indeed, even when five times the amount of KOtf (5 mg) was added to the

Co(PyPc)+K/C cathode, electrocatalytic $CO_2$ reduction was maintained for seven days (Figure S7) without any salt precipitation. Even after a longer period of time (over 500h), no salt precipitation was observed in our system, and the catalytic activity remained stable (Figure S8).

In trials without KOtf addition, the Co(PyPc)/C electrode exhibited poor $CO_2$ reduction activity along with low durability, and the requirement for a high cell voltage (Figure S9). The FE(CO) was also found to decrease from 95% to 50% within 4 h and the cell voltage remained above 2.1 V in conjunction with a current density of -100 mA/cm$^2$. These results indicated that K$^+$ played a very important role in $CO_2$ reduction over the Co(PyPc)/C in the MEA cell because the Co(PyPc)+K/C electrode was able to show continuous $CO_2$ reduction activity for more than 168 h with a cell voltage of less than -2.0 V after incorporating KOtf. This work confirmed that the durability of Co(PyPc) was increased by adding other salts such as potassium perfluoro-1-butanesulfonate (KC$_4$F$_9$Otf) and sodium triflate (NaOtf) (Figures S10 and S11), and the $CO_2$ reduction activities of these systems were also maintained over a period of 24 h. These results indicated that the $CO_2$ reduction activity of the Co(PyPc) could be improved not only by the addition of KOtf but also by incorporating other potassium and sodium salts (Table S2). Our prior work demonstrated that the $CO_2$ reduction activities of catalysts made from Mn, Co and Re-based complexes in aqueous solutions could be enhanced by a synergistic effect obtained by incorporating both K$^+$ and carbon (20). This previous research showed that K$^+$ decreases the activation energy required for $CO_2$ reduction when using metal complex catalysts and so it was concluded that the overpotential for $CO_2$ reduction in the MEA cell was decreased by the K$^+$ effect. The K$^+$ effect for improving the durability was followed by in situ X-ray absorption near edge structure (XANES) spectra (Figure 4). This result clearly showed that the potassium salt in the catalyst layer prevented structural changes in the Co(PyPc) catalyst during electrolysis. If there are no potassium salt in the catalytic layer, it turned into a metal like structure. We confirmed whether the effect of K$^+$ effect could be applied to other catalysts. As a result, the $CO_2$ reduction activity of the Co(Pc) was also improved by adding KOtf (Figure S12). In previous research, the Co(Pc) catalyst was deactivated within several hours at a current density of -100 mA/cm$^2$ (14), while the present work showed that adding KOtf allowed CO production to persist for 24 h with a reaction current of -100 mA/cm$^2$. The cell voltage was also decreased from approximately -2.7 to -2.1 V even with small amounts of Co(Pc) (0.18 mg/cm$^2$) loaded on the carbon layer. These results indicated that the presence of K$^+$ and carbon provided a synergistic effect that improved the durability of the material while also decreasing the cell voltage required for $CO_2$ reduction in an MEA cell with metal complex catalysts.

Recently, the mechanism by which Co tetraphenylporphyrin (CoTPP) is deactivated during electrolytic $CO_2$ reduction was established by experimental work and DFT calculations (28). One of the main reasons for the deactivation of Co(TPP) was found to be off-center binding of $CO_2$ on the complex structure. In fact, the off-center binding of $CO_2$ via carbon atoms is thermodynamically favored over the adsorption of $CO_2$ on the Co atom of the complex following two-electron reduction. It is possible that the Co(PyPc) catalyst was also deactivated via an off-center binding structure because tetraphenylporphyrin and phthalocyanine are very similar groups comprising tetrapyrrole macrocycles. For this reason, the DFT calculations were performed for Co(PyPc) with $CO_2$ as with the prior work (28). In the case of the Co(PyPc) catalyst, the off-center binding of $CO_2$ was also more stable than the adsorption of $CO_2$ on the Co atom of a two-electron-reduced species (Figure S13). However, these same calculations confirmed that the adsorption of $CO_2$ on the Co atoms was preferred following the addition of K$^+$ (Figure S13 red line). The Co(Pc) catalyst also showed similar DFT results to the Co(PyPc)

(Figure S14). Therefore, it appears that decomposition resulting from the off-center binding of $CO_2$ can be prevented by adding a $K^+$ salt to the catalyst layer in the MEA cell, because the adsorption of $CO_2$-$K^+$ on the Co atom is thermodynamically favored over the off-center binding of $CO_2$ structure.

The source of the carbon incorporated in the CO that was generated was assessed by isotope tracer analyses using $^{13}CO_2$ with the Co(PyPc)+K/C electrode (Figure S15). CO with an m/z of 29 was found to be the main product, confirming that the CO detected in these electrocatalytic reactions over Co(PyPc) did not originate from other carbon sources, such as the carbon black.

In summary, the potassium salt in the MEA cell prevented structural changes in Co complex catalysts and lowered the cell overpotential, leading to increased current densities and high durability together with low cell voltages. The cell voltage required for electrochemical $CO_2$ reduction over the Co(PyPc)+K/C in the MEA cell was lowered to -1.59 V when using KOtf as an additive, and the long-term stability of the reductive reaction was improved such that the reaction proceeded for seven days at 100 mA/cm$^2$. As a result, the TON for CO production was over 3,800,000. The Co(PyPc)+K/C in the MEA cell was also shown to function even at 200 mA/cm$^2$ to produce CO. The effect by which $K^+$ significantly enhanced the $CO_2$ reduction reaction rate along with the stability of the Co(PyPc)/C was also applicable to other catalysts such as Co(Pc). Furthermore, the $CO_2$ reduction activity could be improved by adding other potassium and sodium salts. Therefore, this concept could potentially be used in conjunction with other electrocatalysts for $CO_2$ reduction. This type of process could also be a pivotal aspect of developing robust flow cell systems for solar-driven $CO_2$ reduction to produce organic chemicals using low input energy levels and only Earth-abundant materials. The present materials are promising electrochemical catalysts capable of functioning at a current density of 200 mA/cm$^2$ with over 60% energy conversion efficiency during CO production under constant-current conditions. Of course, there is a need to increase the current density, assess the durability of these catalysts over longer time spans (up to several years) and solves anolyte crossover of the MEA cell. Especially, the anolyte crossover when using a KOH solution needs to be solved. This problem could be solved by using neutral solvents or by developing new anion exchange membranes. The Co(PyPc) can act as a catalyst for $CO_2$ reduction even in neutral solvents (Figure S16, in KHCO$_3$), but the anode electrode requires the use of IrOx catalyst because Ni+Fe/Ni catalysts do have not enough stability in the neutral solvents such as KHCO$_3$. Although the Co(PyPc)+K/C electrode has the highest energy conversion efficiency at 50 mA/cm$^2$ in a KHCO$_3$ solution than other catalysts (Table S3), the energy conversion efficiency was decreased than using the KOH solution. One of the main reasons that water oxidation activity was decreased at the neutral conditions[29]. Therefore, developing a new catalyst for water oxidation in the neutral condition is also important for the electrocatalytic $CO_2$ reduction using MEA cell. metal complex catalysts can have high durability and energy conversion efficiency for $CO_2$ reduction with an optimized reaction environment. There are still remaining some problems using metal complex catalysts with MEA cells, but the present findings may suggest that such materials could generate organic compounds with commercially viable economics. The reason is that metal complex catalysts can be controlled by varying their ligands and substituents and have high durability and energy conversion efficiency for $CO_2$ reduction with an optimized reaction environment.
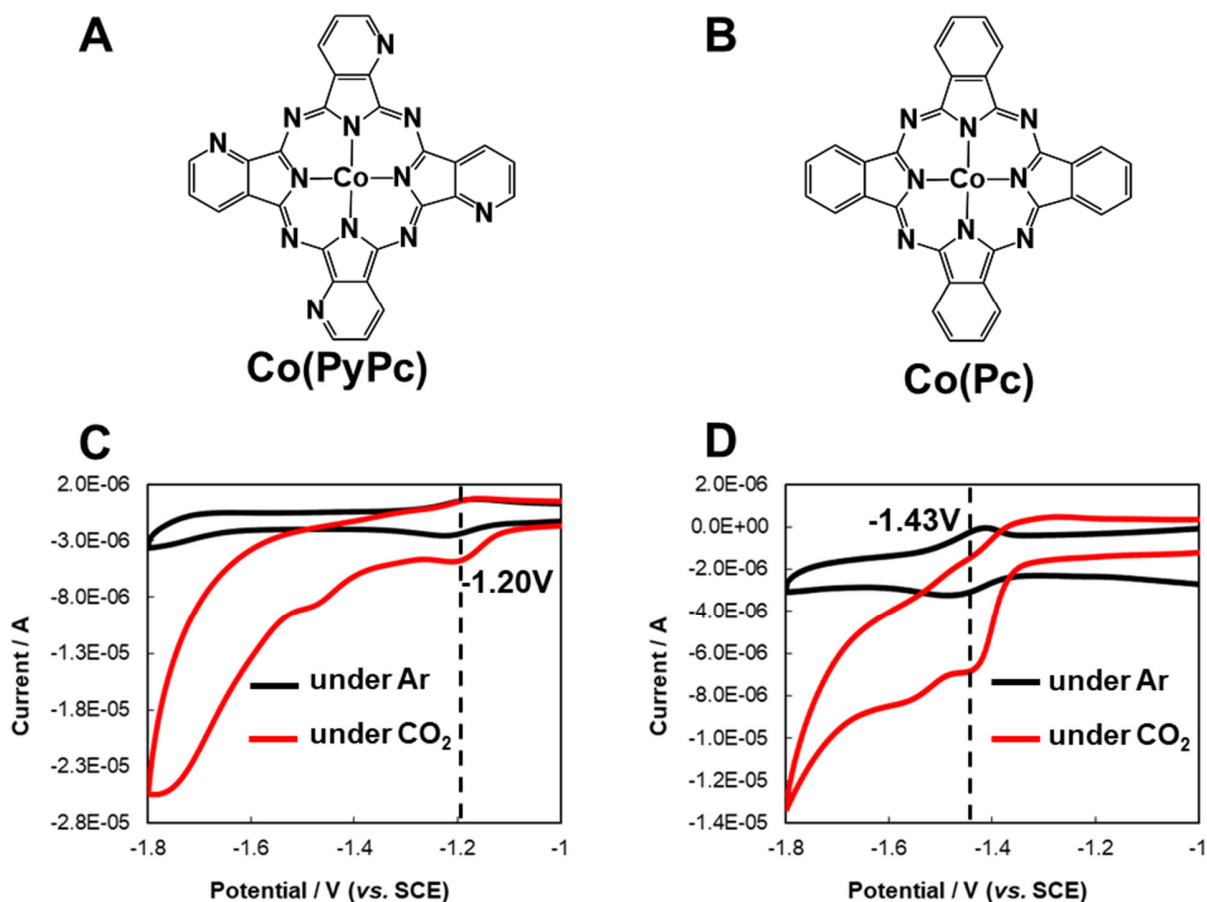
**References and Notes:**

1. W. H. Cheng *et al.*, CO2 Reduction to CO with 19% Efficiency in a Solar-Driven Gas Diffusion Electrode Flow Cell under Outdoor Solar Illumination. *Acs Energy Letters* **5**, 470-476 (2020).

2. Y. Xiao *et al.*, An artificial photosynthetic system with CO2-reducing solar-to-fuel efficiency exceeding 20%. *Journal of Materials Chemistry A* **8**, 18310-18317 (2020).

3. H. A. Schwarz, R. W. Dodson, REDUCTION POTENTIALS OF CO2- AND THE ALCOHOL RADICALS. *J. Phys. Chem.* **93**, 409-414 (1989).

4. A. J. Morris, G. J. Meyer, E. Fujita, Molecular Approaches to the Photocatalytic Reduction of Carbon Dioxide for Solar Fuels. *Accounts Chem. Res.* **42**, 1983-1994 (2009).

5. Y. Hori, K. Kikuchi, S. Suzuki, PRODUCTION OF CO AND CH4 IN ELECTROCHEMICAL REDUCTION OF CO2 AT METAL-ELECTRODES IN AQUEOUS HYDROGENCARBONATE SOLUTION. *Chemistry Letters*, 1695-1698 (1985).

6. P. De Luna *et al.*, What would it take for renewably powered electrosynthesis to displace petrochemical processes? *Science* **364**, eaav3506 (2019).

7. S. Nitopi *et al.*, Progress and Perspectives of Electrochemical CO2 Reduction on Copper in Aqueous Electrolyte. *Chem Rev* **119**, 7610-7672 (2019).

8. S. Verma, X. Lu, S. C. Ma, R. I. Masel, P. J. A. Kenis, The effect of electrolyte composition on the electroreduction of CO2 to CO on Ag based gas diffusion electrodes. *Physical Chemistry Chemical Physics* **18**, 7075-7084 (2016).

9. S. Verma *et al.*, Insights into the Low Overpotential Electroreduction of CO2 to CO on a Supported Gold Catalyst in an Alkaline Flow Electrolyzer. *Acs Energy Letters* **3**, 193-198 (2018).

10. F. P. G. de Arquer *et al.*, CO2 electrolysis to multicarbon products at activities greater than 1 A cm(-2). *Science* **367**, 661-666 (2020).

11. R. I. Masel *et al.*, An industrial perspective on catalysts for low-temperature CO2 electrolysis. *Nat Nanotechnol* **16**, 118-128 (2021).

12. S. S. Bhargava *et al.*, Decreasing the Energy Consumption of the CO2 Electrolysis Process Using a Magnetic Field. *ACS Energy Letters* **6**, 2427-2433 (2021).

13. D. Wakerley *et al.*, Gas diffusion electrodes, reactor designs and key metrics of low-temperature CO2 electrolysers. *Nature Energy* **7**, 130-143 (2022).

14. S. Ren *et al.*, Molecular electrocatalysts can mediate fast, selective CO2 reduction in a flow cell. *Science* **365**, 367-369 (2019).

15. X. Lu *et al.*, High-Performance Electrochemical CO2 Reduction Cells Based on Non-noble Metal Catalysts. *Acs Energy Letters* **3**, 2527-2532 (2018).

16. J. Su *et al.*, Building a stable cationic molecule/electrode interface for highly efficient and durable CO2 reduction at an industrially relevant current. *Energy & Environmental Science* **14**, 483-492 (2021).

17. X. Zhang *et al.*, Molecular engineering of dispersed nickel phthalocyanines on carbon nanotubes for selective CO2 reduction. *Nature Energy* **5**, 684-692 (2020).

18. B. Siritanaratkul *et al.*, Zero-Gap Bipolar Membrane Electrolyzer for Carbon Dioxide Reduction Using Acid-Tolerant Molecular Electrocatalysts. *J Am Chem Soc* **144**, 7551-7556 (2022).

19. H. Takeda, C. Cometto, O. Ishitani, M. Robert, Electrons, Photons, Protons and Earth-Abundant Metal Complexes for Molecular Catalysis of CO2 Reduction. *ACS Catalysis* **7**, 70-88 (2016).

20. S. Sato, K. Saita, K. Sekizawa, S. Maeda, T. Morikawa, Low-Energy Electrocatalytic CO2 Reduction in Water over Mn-Complex Catalyst Electrode Aided by a Nanocarbon Support and K+ Cations. *ACS Catalysis* **8**, 4452-4458 (2018).

21. E. Villagra *et al.*, Tuning the redox properties of Co-N4 macrocyclic complexes for the catalytic electrooxidation of glucose. *Electrochimica Acta* **53**, 4883-4888 (2008).

22. C. Linares-Flores *et al.*, Reinterpreting the Role of the Catalyst Formal Potential. The case of Thiocyanate Electrooxidation Catalyzed by CoN4-Macrocyclic Complexes. *Journal of Physical Chemistry C* **116**, 7091-7098 (2012).

23. K. Koike *et al.*, Key process of the photocatalytic reduction of CO2 using Re(4,4 '-X-2-bipyridine)(CO)(3)PR3 (+) (X = CH3, H, CF3; PR3 = phosphorus ligands): Dark reaction of the one-electron-reduced complexes with CO2. *Organometallics* **16**, 5724-5729 (1997).

24. T. M. Suzuki *et al.*, Highly Enhanced Electrochemical Water Oxidation Reaction over Hyperfine β-FeOOH(Cl):Ni Nanorod Electrode by Modification with Amorphous Ni(OH)2. *Bulletin of the Chemical Society of Japan* **91**, 778-786 (2018).

25. T. Arai, S. Sato, K. Sekizawa, T. M. Suzuki, T. Morikawa, Solar-driven CO2 to CO reduction utilizing H2O as an electron donor by earth-abundant Mn-bipyridine complex and Ni-modified Fe-oxyhydroxide catalysts activated in a single-compartment reactor. *Chemical Communications* **55**, 237-240 (2019).

26. L.-C. Weng, A. T. Bell, A. Z. Weber, Towards membrane-electrode assembly systems for CO2 reduction: a modeling study. *Energy & Environmental Science* **12**, 1950-1968 (2019).

27. D. G. Wheeler *et al.*, Quantification of water transport in a CO2 electrolyzer. *Energy & Environmental Science* **13**, 5126-5134 (2020).

28. A. N. Marianov *et al.*, Resolving Deactivation Pathways of Co Porphyrin-Based Electrocatalysts for CO2 Reduction in Aqueous Medium. *ACS Catalysis* **11**, 3715-3729 (2021).

29. Y. Dong, C. W. Oloman, E. L. Gyenge, J. Su, L. Chen, Transition metal based heterogeneous electrocatalysts for the oxygen evolution reaction at near-neutral pH. *Nanoscale* **12**, 9924-9934 (2020).

**Fig. 1.** Molecular structures of the (A) Co(PyPc) and (B) Co(Pc) electrocatalysts. Cyclic voltammograms obtained from (C) Co(PyPc) and (D) Co(Pc) in DMF containing 0.1 M NEt$_4^+$BF$_4^-$ under Ar (black) and under CO$_2$ (red). Measurements were conducted using a glassy carbon working electrode, a Pt counter electrode and an Ag/AgNO$_3$ reference electrode at a scan rate of 50 mVs$^{-1}$.
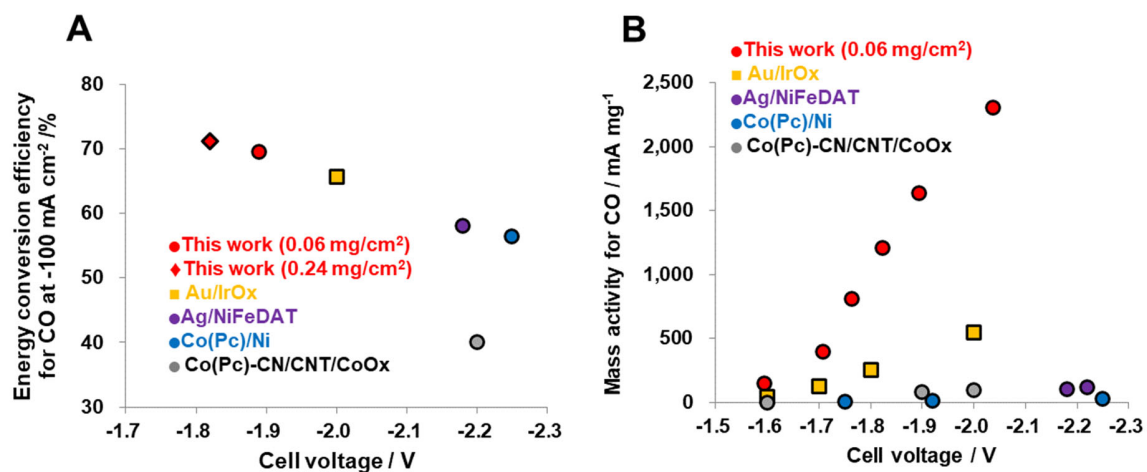
**Fig. 2.** Comparisons of the results reported in this work (red) with the literature data (yellow (*9*), purple (*12*), blue (*14*) and gray (*15*)) in terms of (A) the energy conversion efficiency during CO production at -100 mA/cm$^2$ and (B) mass-based activity as a function of the cell potential without resistance compensation in conjunction with water oxidation using a KOH solution at room temperature.
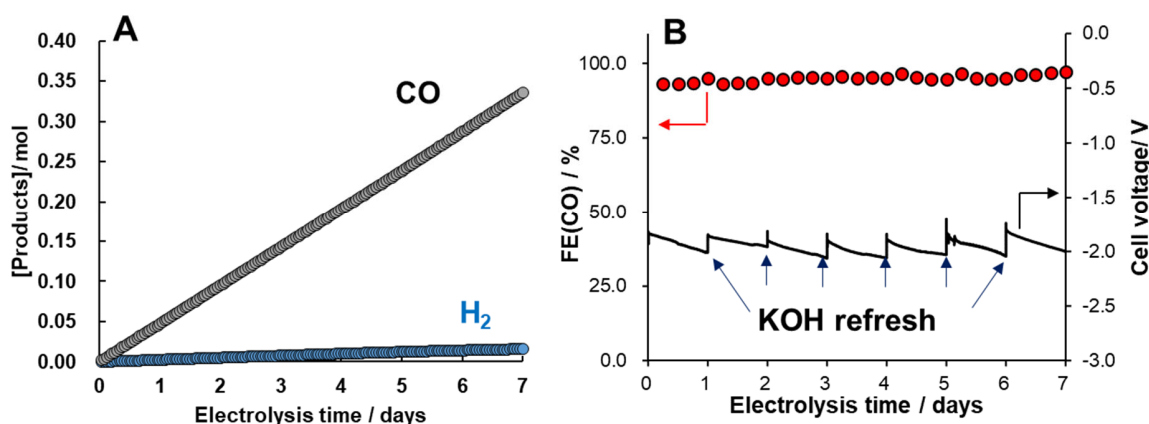


**Fig. 3.** Electrocatalytic activity of the Co(PyPc)+K/C electrode using the MEA cell during long-term bulk electrolysis at -100 mA/cm$^2$. (A) Moles of CO (black) and H$_2$ (blue) produced using the Co(PyPc)+K/C electrode loaded with 0.05 mg of Co(PyPc) and (B) Faradaic efficiency during CO production (FE(CO), red circles) and cell potential at a constant current density of -100 mA/cm$^2$ (black line).
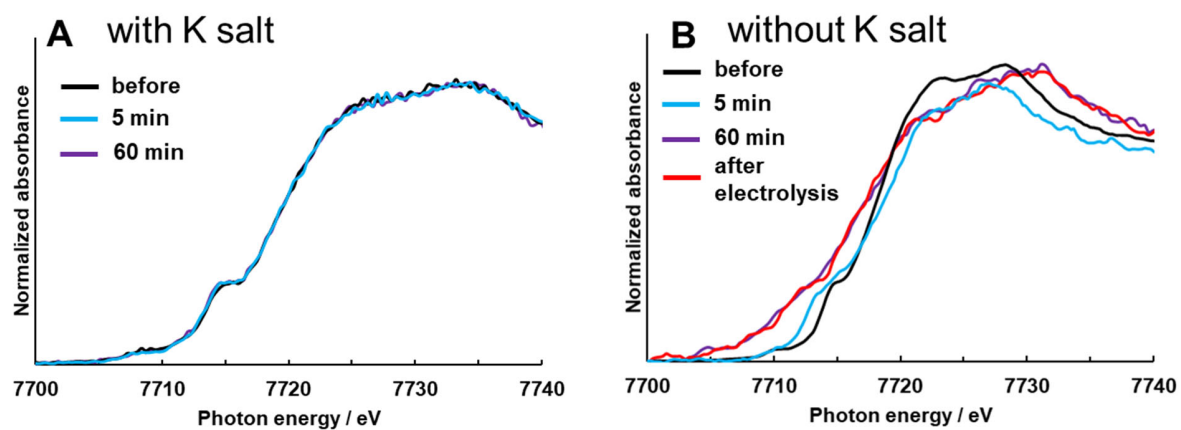
**Fig. 4.** *In situ* XANES spectra of (A) Co(PyPc)+K/C and (B) Co(PyPc)/C electrodes at -1.4 V (vs Ag/AgCl) under $CO_2$ [before electrolysis (black), 5 min electrolysis (blue), 60 min electrolysis (purple) and after electrolysis (red)].

5

**Table 1.** Summary of the results obtained from electrocatalytic $CO_2$ reduction trials using the Co(PyPc)+K/C electrode loaded with 0.06 mg of Co(PyPc) with the MEA cell for 2 h at various constant current densities.*

| Current density / mA cm$^{-2}$ | Cell voltage** / V | FE(CO) / % | Mass activity for CO** /mA mg$^{-1}$ | Energy conversion efficiency** / % |
|---|---|---|---|---|
| -10 | -1.59 | 90.8 ± 4.4 | 151.3 | 76.4 |
| -25 | -1.71 | 94.3 ± 3.2 | 392.9 | 74.0 |
| -50 | -1.76 | 97.4 ± 1.3 | 811.7 | 74.0 |
| -75 | -1.82 | 96.8 ± 3.2 | 1210.0 | 71.2 |
| -100 | -1.89 | 98.2 ± 1.0 | 1636.7 | 69.5 |
| -150 | -2.04 | 92.3 ± 0.5 | 2307.5 | 60.7 |
| -50*** | -1.71 | 95.5 ± 0.5 | 191.9 | 74.8 |
| -100*** | -1.82 | 96.7 ± 2.9 | 402.9 | 71.2 |
| -150*** | -1.91 | 95.3 ± 2.1 | 595.6 | 66.8 |
| -200*** | -2.03 | 95.2 ± 3.6 | 793.3 | 62.8 |

*All chronopotentiometry data are provided in Figures S17 and 18.

** These data represent averages over the 2 h reaction time span.

*** In these trials 0.24 mg Co(PyPc) was loaded on the electrode.

## Supplementary Materials

### Materials

Reagents and solvents were purchased from FUJIFILM Wako Pure Chemical, Kanto Chemical, Tokyo Kasei and Aldrich and used without further purification. Carbon fiber paper (AVcarb 3520) was purchased from AvCarb Material Solutions.

### General procedures

The redox potentials of the complexes were determined in dimethyl formamide (DMF) containing tetraethylammonium tetrafluoroborate ($NEt_4^+BF_4^-$, 0.1 M) as a supporting electrolyte using cyclic voltammetry with an ALS/CHI CHI-620 electrochemical analyzer. These trials employed a glassy carbon disk working electrode (3 mm diameter), $Ag/AgNO_3$ (0.1 M) reference electrode and Pt counter electrode. The supporting electrolyte ($NEt_4^+BF_4^-$) was dried under vacuum at 373 K for one day prior to use. The molecular structures of the complexes were determined by time-of-flight mass spectrometry (TOFMS, Jeol JMS-T100LP) with methanol as the mobile phase. A potentiostat/galvanostat (SP-150, Bio-Logic Science Instruments) was used during the electrochemical catalytic reaction trials with the membrane electrode assembly (MEA) cell system. Gaseous reaction products, such as CO and $H_2$, were analyzed using a gas chromatograph (GC) (Micro GC Fusion 3, INFICON). The amounts of each Co complex loaded on the carbon substrates were determined by inductively coupled plasma (ICP) analyses (Rigaku, CIROS 120 EOP). Transmission electron microcopy (TEM) images were obtained using a JEM-2100F instrument (Jeol) at an acceleration voltage of 200 kV. Co 2p and N 1s X-ray photoelectron spectroscopy (XPS data were acquired using a Quantera SXM instrument (ULVAC-PHI) with monochromated Al Kα radiation. Anion exchange membrane(AEM) and IrOx were synthesized according to a previously reported method(*25*).

### Fabrication of Co(PyPc)+K/C electrodes containing 0.05 or 0.06 mg Co(PyPc)

The cobalt-tetrapyridino-porphyrazine (Co(PyPc)) catalyst was synthesized according to a previously reported method (*1*). Electrodes were fabricated by adding 60 mg carbon black (Vulcan XC 72R) to 40 ml DMF followed by sonication for 30 min, after which 2 mg Co(PyPc) was added followed by sonication for an additional 30 min. The sonicated solution was subsequently stirred for 24 h at room temperature after which the resulting carbon black with Co(PyPc) was collected by filtration, washed with DMF and ethanol and then dried in air. The Co(PyPc) loading in the product was assessed by ICP and determined to be 0.02 mg Co(PyPc)/1 mg carbon. Subsequently, 10 mg of this carbon black with Co(PyPc), 1 mg potassium triflate (KOtf) and 0.1 ml of a Nafion solution were added to 0.9 ml ethanol. The resulting mixture was sonicated for 5 min and then agitated using a vortex mixer. A 0.05 ml quantity of this dispersion was then applied to a AVcarb 3520 substrate having a surface area of 1.13 $cm^2$ and dried at 333 K for 5 min. This coating procedure was repeated five or six times so as to load either 0.05 or 0.06 mg of the Co(PyPc) onto the AVcarb, respectively. The resulting Co(PyPc)+K/C electrodes were allowed to stand in the dark at 333 K overnight.

### Fabrication of a Co(PyPc)+K/C electrode containing 0.24 mg Co(PyPc)

The Co(PyPc) catalyst was synthesized according to a previously reported method (*1*). Electrodes were synthesized by adding 60 mg carbon black (Vulcan XC 72R) to 40 ml DMF followed by sonication for 30 min. Following this, 10 mg of the Co(PyPc) was added with sonication for a further 30 min, after which the dispersion was stirred for 24 h at room

temperature. The resulting carbon black with Co(PyPc) was collected by filtration and washed with DMF and EtOH then dried in air. The Co(PyPc) loading was confirmed by ICP analysis to be 0.08 mg Co(PyPc)/1 mg carbon.

Subsequently, 10 mg of the carbon black with Co(PyPc), 1 mg KOtf and 0.1 ml of a Nafion solution were added to 0.9 ml ethanol and the mixture was sonicated for 5 min followed by agitation with a vortex mixer. A 0.05 ml quantity of this mixture was applied to an AVcarb 3520 substrate having a surface area of 1.13 cm$^2$ and then dried at 333 K for 5 min. This procedure was repeated six times to deposit a total of 0.24 mg of the Co(PyPc) on the substrate and the resulting Co(PyPc)+K/C electrode was allowed to stand in the dark at 333 K overnight.

### Fabrication of a Co(PyPc)/C electrode

A 10 mg quantity of the carbon black with Co(PyPc) and 0.1 ml of a Nafion solution were added to 0.9 ethanol and the dispersion was sonicated for 5 min and then agitated with a vortex mixer. A 0.05 ml portion of this mixture was dropped onto an AVcarb 3520 substrate having a surface area of 1.13 cm$^2$ and then dried at 333 K for 5 min. This coating procedure was repeated six times to load a total of 0.06 mg of the Co(PyPc) on the substrate and the resulting Co(PyPc)/C electrode was then allowed to stand in the dark at 333 K overnight.

### Fabrication of a Co(Pc)+K/C electrode

The cobalt phthalocyanine (Co(Pc)) catalyst was synthesized according to a previously reported method (1). The electrode was fabricated by adding 60 mg carbon black (Vulcan XC 72R) to 40 ml DMF followed by sonication for 30 min, after which 10 mg of the Co(Pc) was added followed by sonication for a further 30 min. The sonicated dispersion was stirred for 24 h at room temperature, after which the carbon black with Co(Pc) was collected by filtration, washed with DMF and ethanol, and then dried in air. An ICP analysis confirmed that the catalyst loading was 0.06 mg Co(Pc)/1 mg carbon.

A 10 mg quantity of the carbon black with Co(Pc), 1 mg KOtf and 0.1 ml of a Nafion solution were added to 0.9 ml ethanol and the mixture was sonicated for 5 min followed by agitation with a vortex mixer. A 0.05 ml portion of this mixture was subsequently dropped onto an AVcarb 3520 substrate (1.13 cm$^2$) and dried at 333 K for 5 min. This coating procedure was repeated six times to deposit a total of 0.18 mg of the Co(Pc) on the AVcarb. The resulting Co(Pc)+K/C electrode was allowed to stand in the dark at 333 K overnight.

### Fabrication of a Co(PyPc)+KC$_4$F$_9$Otf/C electrode

A 10 mg quantity of the carbon black with Co(PyPc), 1 mg potassium perfluoro-1-butanesulfonate (KC$_4$F$_9$Otf) and 0.1 ml of a Nafion solution were added to 0.9 ml ethanol and the dispersion was sonicated for 5 min and then agitated using a vortex mixer. A 0.05 ml quantity of this dispersion was subsequently dropped onto an AVcarb 3520 substrate (1.13 cm$^2$) and then dried at 333 K for 5 min. This coating procedure was repeated six times to load a total of 0.06 mg of the Co(PyPc) on the AVcarb. The resulting Co(PyPc)+ KC$_4$F$_9$Otf /C electrode was allowed to stand in the dark at 333 K overnight.

### Fabrication of a Co(PyPc)+NaOtf/C electrode

A 10 mg quantity of the carbon black with Co(PyPc), 1 mg sodium triflate (NaOtf) and 0.1 ml of a Nafion solution were added to 0.9 ethanol and the dispersion was sonicated for 5 min and then agitated using a vortex mixer. A 0.05 ml quantity of this mixture was subsequently dropped onto

an AVcarb 3520 substrate (1.13 cm$^2$) and then dried at 333 K for 5 min. This coating procedure was repeated six times to load a total of 0.06 mg of the Co(PyPc) on the AVcarb. The resulting Co(PyPc)+NaOtf/C electrode was allowed to stand in the dark at 333 K overnight.

**Fabrication of a Ni+Fe/Ni electrode**
The Ni-doped β-FeOOH catalyst was synthesized according to a previously reported method (*2*), after which 10 ml of an aqueous dispersion solution of the Ni-doped β-FeOOH, 150 mg NiCl$_2$·6H$_2$O and 75 mg FeCl$_2$·4H$_2$O were added to 10 ml pure water. A section of Ni foam was dipped into the resulting mixture and then calcined at 423 K for 2 h under air. Finally, pre-electrolysis was conducted at +0.60 V (vs. Ag/AgCl) for 1 h in a 1.0 M KOH solution, after which the Ni+Fe/Ni electrode was cut to provide a specimen with a surface area of 1.13 cm$^2$.

**Electrocatalytic reaction**
The MEA cell electrolyzer (Carbon Dioxide Electrolyzer® purchased from Dioxide Materials) was composed of two flow plates, the sample and Ni+Fe/Ni or IrOx electrodes (each with a surface area of 1.13 cm$^2$), Teflon spacers and an AEM. A diagram of the MEA cell is provided in Figure S1. Wet CO$_2$ was fed to the cathode at 100 standard cubic centimeters per minute (SCCM) while a recirculated 1 M KOH solution or 0.2 M KHCO$_3$ was fed to the anode at a flow rate of 100 ml/min. The cell was equipped with an autosampler to allow for *in situ* measurements and was directly connected to a GC (Micro GC Fusion 3) for the analysis of CO and H$_2$ using a thermal conductivity detector at 20 min intervals. A potentiostat/galvanostat (SP-150, Bio-Logic Science Instruments) was used for electrochemical measurements. All applied potentials and voltages were determined without iR compensation.

**Computational Details.**
The effects of the potassium cation (K$^+$) on the CO$_2$ adsorption to a Co(PyPc) were examined using quantum chemical calculations. Changes in free energy for the CO$_2$ adsorption reactions (1) and (2) ($\Delta G_{ads}$) were calculated using the density functional theory (DFT) method to focus on the effects of the K$^+$ cation. In these reactions, adsorption of the carbon atom of the CO$_2$ molecule to the central Co atom was assumed. Henceforth, this type of adsorption is denoted as on-center binding.

$$[Co(PyPc)]^{2-} \quad + \quad CO_2 \quad \rightarrow \quad [Co(PyPc)(CO_2)]^{2-} \quad (1)$$
$$[Co(PyPc)K]^{2-} \quad + \quad CO_2 \quad \rightarrow \quad [Co(PyPc)(CO_2)K]^{2-} \quad (2)$$

Regarding the off-center binding of CO$_2$, the following a reaction (3) were examined.

$$[Co(PyPc)]^{-} \quad + \quad CO_2 \quad \rightarrow \quad [Co(PyPc)\{OC(=O)\}]^{2-} \quad (3)$$

The same reactions for a Co(Pc) were also assumed and calculated for comparison. The molecular geometrical structure of each species was optimized, and its Gibbs free energy at the optimized structure was obtained by carrying out vibrational analysis. The *ω*B97XD functional (*3*) was adopted for the DFT calculations. The basis set with relativistic compact effective potentials by W. J. Stevens et al. was used for the Co atoms (*4*), while the 6-31G(d,p) basis set (*5-8*) was used for other elements. Solvent effects of water were incorporated into the

calculations by adopting the polarizable continuum model (PCM) (*9-14*). All the calculations were carried out using the Gaussian16 program (*15*).

The calculated Gibbs free energies and $\Delta G_{ads}$ values are summarized in Table S4. The calculated $\Delta G_{ads}$ values for reaction (1) was positively high, indicating that the on-center binding is energetically unfavorable in the absence of the $K^+$ cation for Co(PyPc). In contrast, $\Delta G_{ads}$ for reaction (2) is reduced from that of reaction (1). This result suggests that the $K^+$ cation stabilizes the $CO_2$ adsorbed structures to promote the on-center binding; the effect is more significant for highly reduced species. Figure S19 shows the Corey–Pauling–Koltun (CPK) space-filling model of $[Co(PyPc)(CO_2)K]^{2-}$. The models show that the $K^+$ cation interacts with not only the adsorbed $CO_2$ molecule but the phthalocyanine ring because of its large ionic radius (*16*), which is responsible for the stabilization of these species. This effect of the $K^+$ cation is similar to that computationally analyzed in the $CO_2$ reduction with the Mn-complex catalyst; the interaction of the $K^+$ cation with the adsorbed $CO_2$ molecule stabilizes the transition state and lowers the reaction barrier (*17*).

The optimized molecular structure of $[Co(Pc)\{OC(=O)\}]^{2-}$ is shown in Figure S20. The off-center binding of $CO_2$ was observed for $[Co(PyPc)\{OC(=O)\}]^{2-}$; the $CO_2$ molecule was adsorbed on one of the carbon atoms neighboring pyrrole nitrogen atoms, and the phthalocyanine ring was distorted from a planar structure. The calculated $\Delta G_{ads}$ for reaction (3) was -4.9 kJ/mol, which is remarkably reduced from $\Delta G_{ads}$ for reaction (1) to a negative value. The results suggest that, in the absence of $K^+$, the off-center binding of $CO_2$ to a highly reduced Co(PyPc) is a preferable process to the on-center binding. Figure S20 shows that the $K^+$ cation occupies one of the off-center-binding cites. This structural effect could block the off-center binding process, which can be responsible for improving the material's durability.

The results for Co(Pc) were generally similar to those for Co(PyPc). The on-center binding of $CO_2$ without $K^+$ is energetically unfavorable, as suggested from the calculated $\Delta G_{ads}$ values for reaction (1). In contrast, the $\Delta G_{ads}$ values for reaction (2) was negative, suggesting that the $K^+$ cation stabilizes the $CO_2$ adsorbed structures to promote the on-center binding. The optimized structure for $[Co(Pc)(CO_2)K]^{2-}$ were quite similar to that for $[Co(PyPc)(CO_2)K]^{2-}$, respectively, suggesting the interactions of the $K^+$ cation with both the adsorbed $CO_2$ and phthalocyanine ring (Figure S21). The calculated $\Delta G_{ads}$ of reaction (3) was $-27.3$ kJ/mol, suggesting that the off-center binding of $CO_2$ to $[Co(PyPc)\{OC(=O)\}]^{2-}$ (Figure S22) is a preferable process to the on-center binding.

The $\Delta G_{ads}$ values for the reactions with Co(Pc) were generally lower than those for Co(PyPc). This trend can be attributed to the difference in the electron-donating property. The number of nitrogen atoms in the Pc ring is less than that of the PyPc ring. Therefore, the electron-donating property of Co(Pc) is higher than that of Co(PyPc), which results in stronger binding of the $CO_2$ molecule.

### *in situ* X-Ray absorption spectroscopy

The chemical states of Co were evaluated by X-ray absorption fine structure (XAFS) spectroscopy using the quick-XAFS technique. (*18*) *In-situ* XAFS measurement was performed using a custom-designed two compartment cell in a three-electrode configuration. A **Co(PyPc)+K/C** and **Co(PyPc)/C** electrode were used as the working electrode (WE), a silver/silver chloride (Ag/AgCl) electrode (EC Frontier, RE-T14) as the reference electrode (RE), and a platinum foil (Pt-foil) electrode (Niraco, PT-353212, φ20 mm×0.02 mm, 99.98%) as the counter electrode (CE). The electrolysis *in-situ* XAFS cell for electrocatalytic $CO_2$ reduction

consisted of an anode and a cathode separated by an anion exchange membrane (ASE, Astom Co., Ltd.), together with a $CO_2$-saturated 0.5 M aqueous solution of $KHCO_3$ as the electrolyte. The working electrode has a Kapton film window for fluorescence XAFS measurement. During the *in-situ* XAFS measurement, $CO_2$ was continuously flowed into the working electrode (cathode) side of the cell. Applied potential was controlled by bi-potentiostat (Model 2325, ALS) at −1.4 V (vs. Ag/AgCl).

**Calculation of the Faradaic efficiency and current density associated with CO production during the electroreduction of $CO_2$ to CO**

The Faradaic efficiency for CO production (FE(CO)) was calculated as:

$$FE(CO) (\%) = 2 \times n / F \times Q \times 100,$$

where n is the moles CO, F is Faraday's constant (96,485 C $mol^{-1}$) and Q is the amount of charge passing through the system. The current density associated with CO production (Jco) was calculated as:

$$Jco = \text{current density} \times FE(CO).$$

**Calculation of the energy conversion efficiency for the electroreduction of $CO_2$ to CO**

The energy conversion efficiency for the electroreduction of $CO_2$ to CO was calculated as:

$$\text{Energy conversion efficiency} = FE(CO) \times Ecell° / Ecell,$$

where Ecell° is the thermodynamic equilibrium potential for the reaction from $CO_2$ to CO (1.34 V) and Ecell is the applied cell voltage.
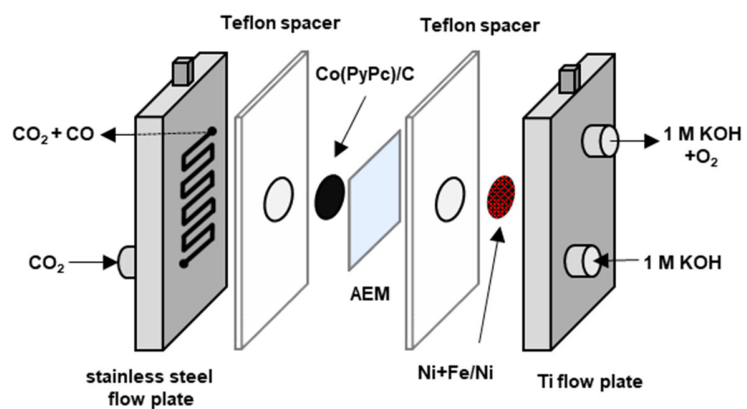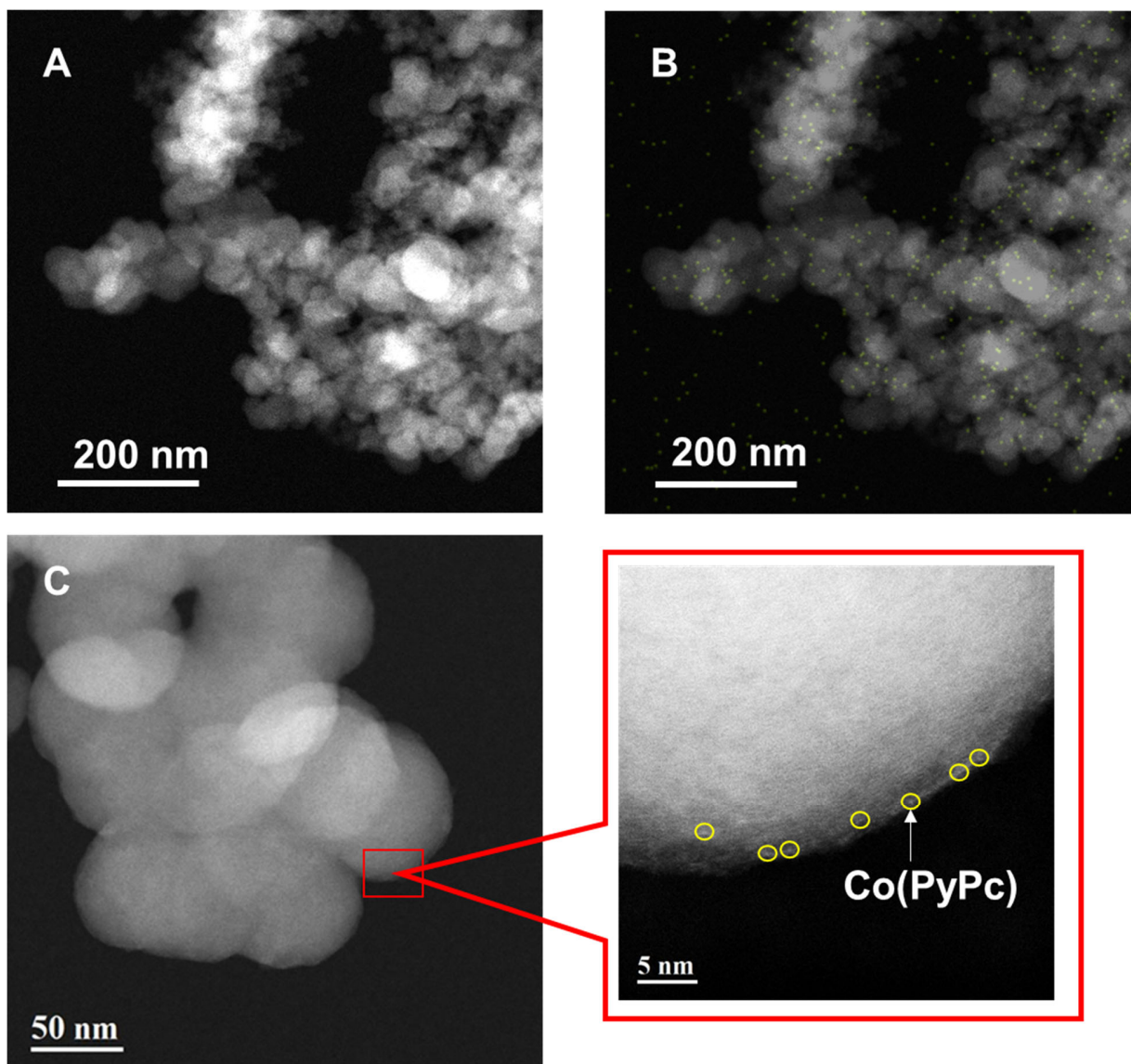
Figure S1. Diagram of the MEA cell.

5

Figure S2. TEM images of the carbon black with Co(PyPc). (A) A typical TEM image, (B) an EDS Co map (in which Co appears as green spots) and (C) a HADDF-STEM image of the carbon black with Co(PyPc). The bright spots in yellow circles in (C) correspond to the central Co atoms of Co(PyPc) complexes.
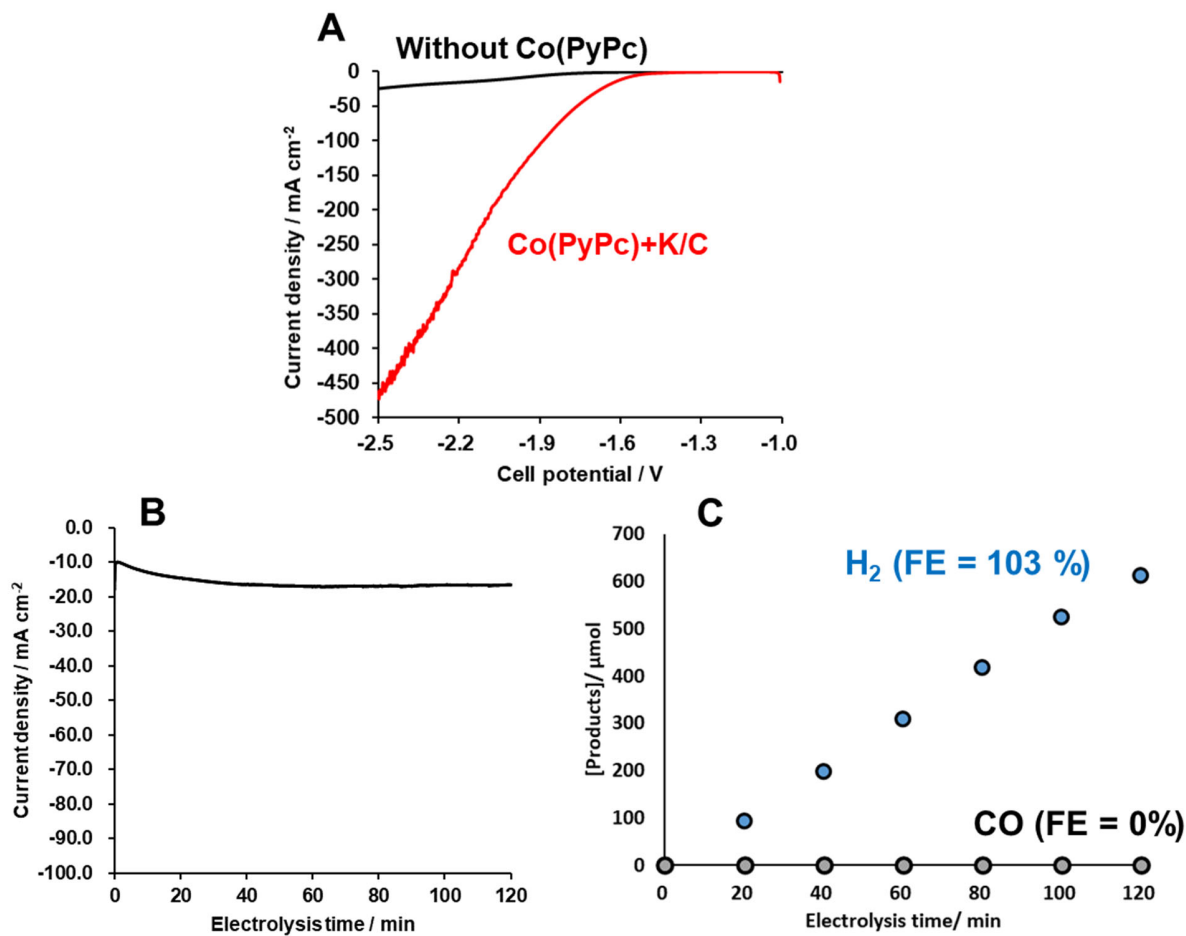
Figure S3. (A) Linear sweep voltammetry data for the K/C (black, without Co(PyPc)) and Co(PyPc)+K/C (red) electrocatalysts obtained using the MEA cell. (B) A chronoamperogram obtained from the K/C electrode during a 2 h electrolysis trial with a -1.9 V cell voltage. (C) Moles of CO (black) and hydrogen (blue) produced using the K/C electrode with the MEA cell, representing measures of the electrocatalytic activity of the material.
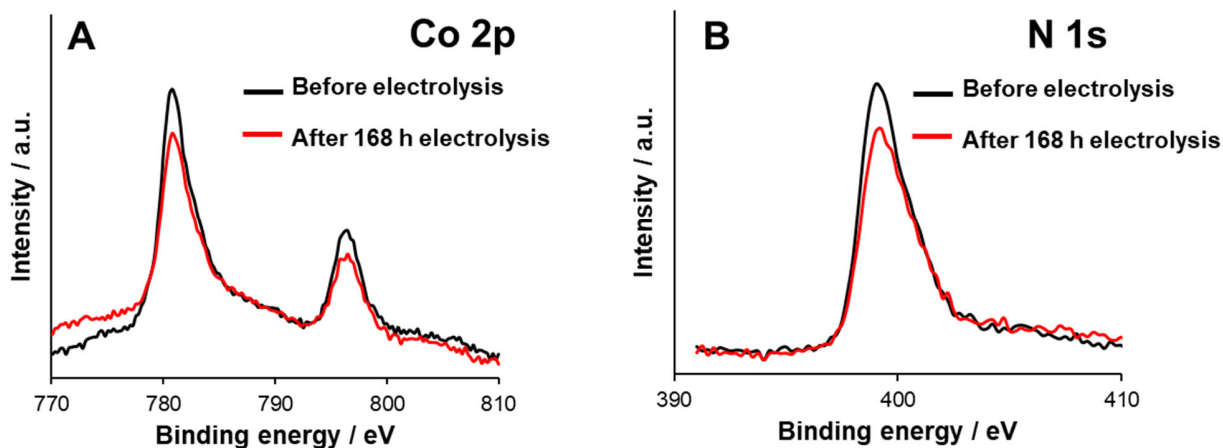
Figure S4. (A) Co 2p and (B) N 1s XPS data obtained from the Co(PyPc)+K/C electrode and after a 168 h electrolysis trial (TON = 3,859,745).
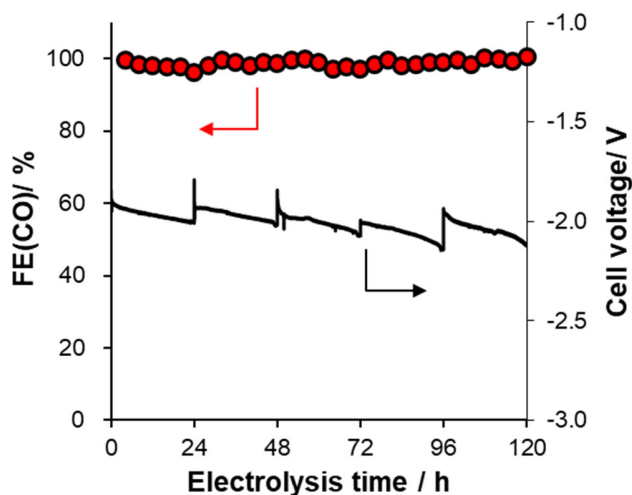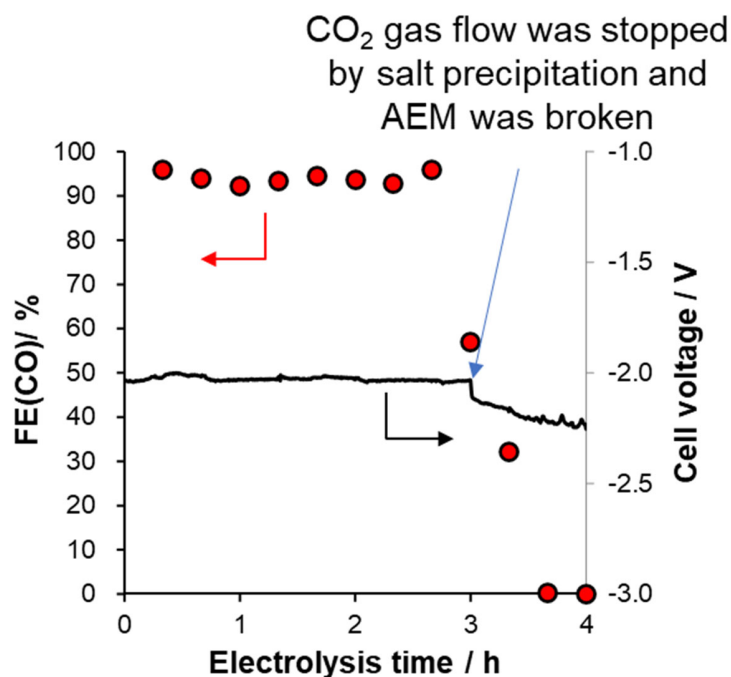


Figure S5. Electrocatalytic activity of the Co(PyPc)+K/C electrode containing 0.24 mg Co(PyPc) using the MEA cell during long-term bulk electrolysis at -150 mA/cm$^2$ as shown by the Faradaic efficiency associated with CO production (FE(CO), red circles) and cell voltage at a constant current density of -150 mA/cm$^2$ (black line). During this trial, the KOH solution was refreshed after every 24 h of electrolysis.

Figure S6. Electrocatalytic activity of the Co(PyPc)+K/C electrode containing 0.24 mg Co(PyPc) using the MEA cell during long-term bulk electrolysis at -200 mA/cm$^2$, as indicated by the Faradaic efficiency for CO production (FE(CO), red circles) and cell voltage at a constant current density of -200 mA/cm$^2$ (black line).
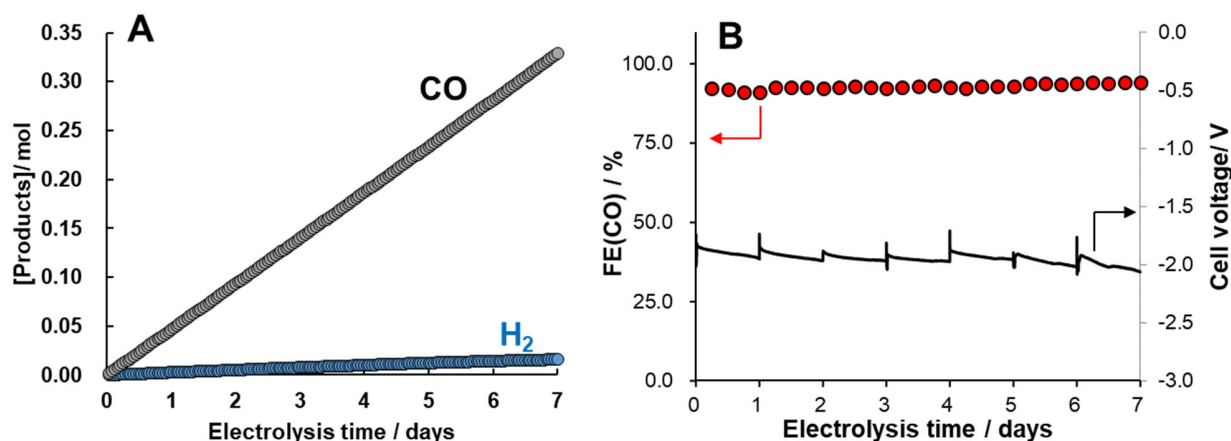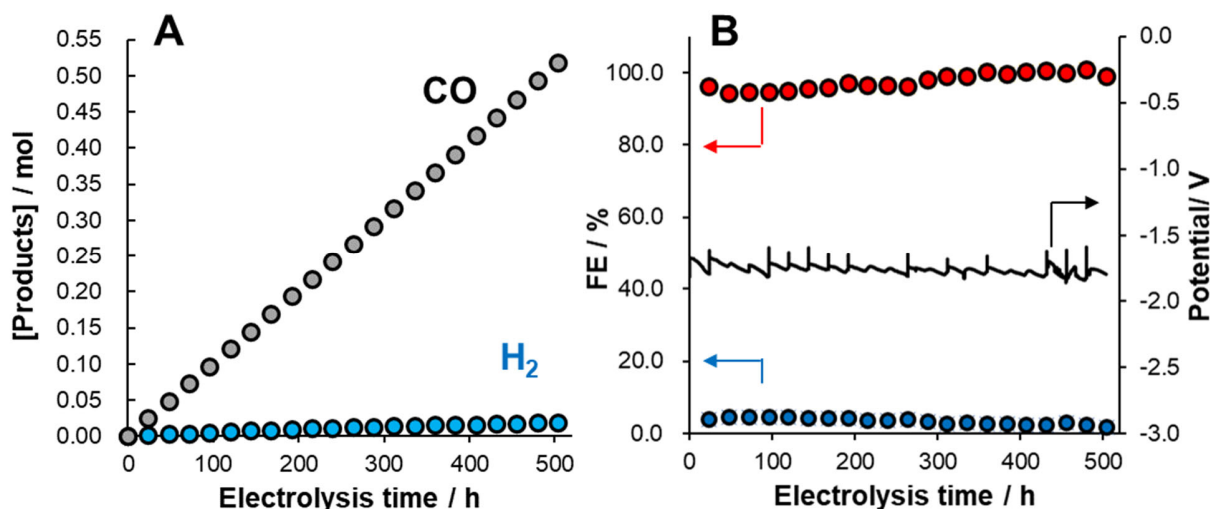


Figure S7. (A) Electrocatalytic activity of the Co(PyPc)+K/C electrode containing 0.05 mg Co(PyPc) and 5 mg KOtf using the MEA cell during long-term bulk electrolysis at -100 mA/cm$^2$ as indicated by the moles of CO (black) and hydrogen (blue) produced. (B) Electrocatalytic activity of the Co(PyPc)+K/C electrode using the MEA cell during long-term bulk electrolysis at -100 mA/cm$^2$ as indicated by the Faradaic efficiency associated with CO production (FE(CO), red circles) and cell voltage at a constant current density of -100 mA/cm$^2$ (black line). During this trial, the KOH solution was refreshed after every 24 h of electrolysis.

Figure S8. (A) Electrocatalytic activity of the Co(PyPc)+K/C electrode containing 0.24 mg Co(PyPc) and 5 mg KOtf using the MEA cell during long-term bulk electrolysis at -50 mA/cm$^2$ as indicated by the moles of CO (black) and hydrogen (blue) produced. (B) Electrocatalytic activity of the Co(PyPc)+K/C electrode using the MEA cell during long-term bulk electrolysis at -50 mA/cm$^2$ as indicated by the Faradaic efficiency associated with CO production (FE(CO), red circles), H$_2$ production (FE(H$_2$), blue circles) and cell voltage at a constant current density of -50 mA/cm$^2$ (black line). During this trial, the KOH solution was refreshed after every 48 or 72 h of electrolysis.
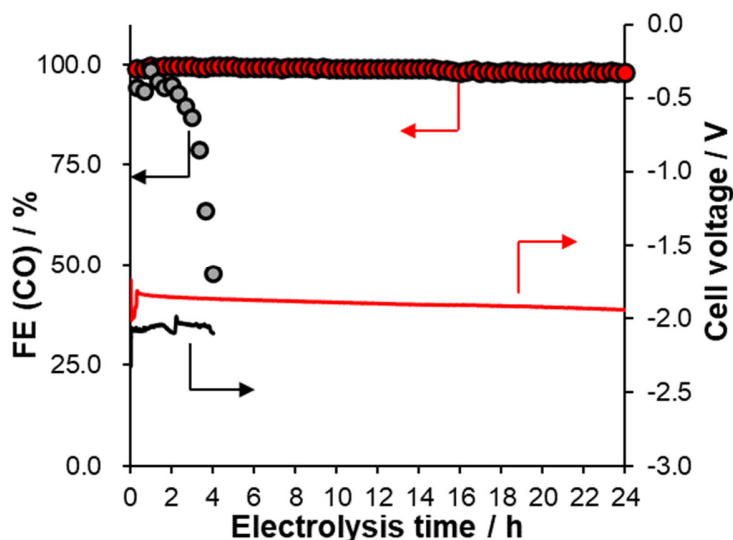


Figure S9. Electrocatalytic activities of the Co(PyPc)/C and Co(PyPc)+K/C electrodes each loaded with 0.06 mg Co(PyPc) using the MEA cell during long-term bulk electrolysis at -100 mA/cm$^2$. Faradaic efficiency for CO production using the Co(PyPc)+K/C (FE(CO), red circles) and Co(PyPc)/C (black circles) and cell voltages at a constant current density of -100 mA/cm$^2$ using the Co(PyPc)+K/C (red line) and Co(PyPc)/C (black line) are shown.
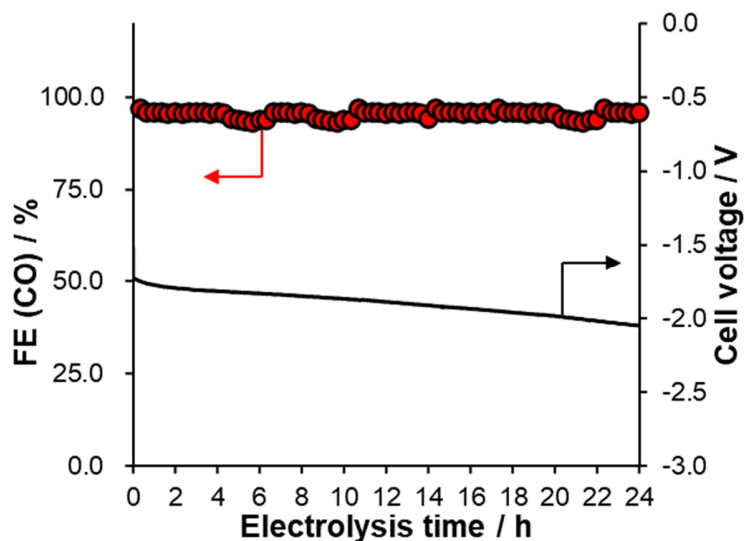
Figure S10. Electrocatalytic activity of the Co(PyPc) + KC$_4$F$_9$Otf/C electrode loaded with 0.06 mg Co(PyPc) using the MEA cell during long-term bulk electrolysis at -100 mA/cm$^2$, as indicated by the Faradaic efficiency for CO production (FE(CO), red circles) and cell voltage at a constant current density of -100 mA/cm$^2$ (black line).
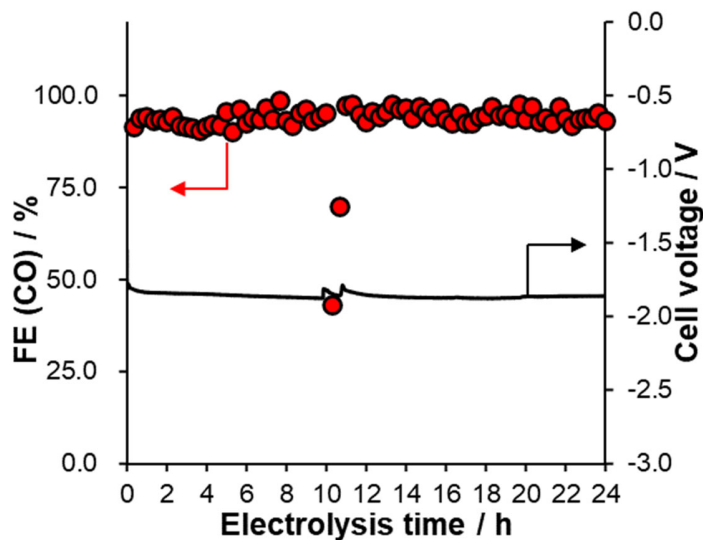


Figure S11. Electrocatalytic activity of the Co(PyPc)+NaOtf/C electrode loaded with 0.06 mg Co(PyPc) using the MEA cell during long-term bulk electrolysis at -50 mA/cm$^2$, as indicated by the Faradaic efficiency for CO production (FE(CO), red circles) and cell voltage at a constant current density of -100 mA/cm$^2$ (black line).
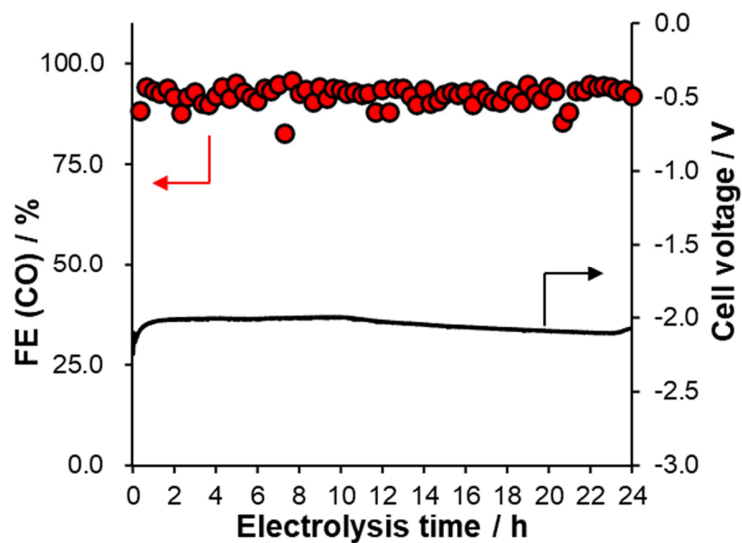
Figure S12. Electrocatalytic activity of the Co(Pc)+K/C electrode loaded with 0.18 mg Co(Pc) using the MEA cell during long-term bulk electrolysis at -100 mA/cm$^2$, as indicated by Faradaic efficiency for CO production (FE(CO), red circles) and cell voltage at a constant current density of -100 mA/cm$^2$ (black line).
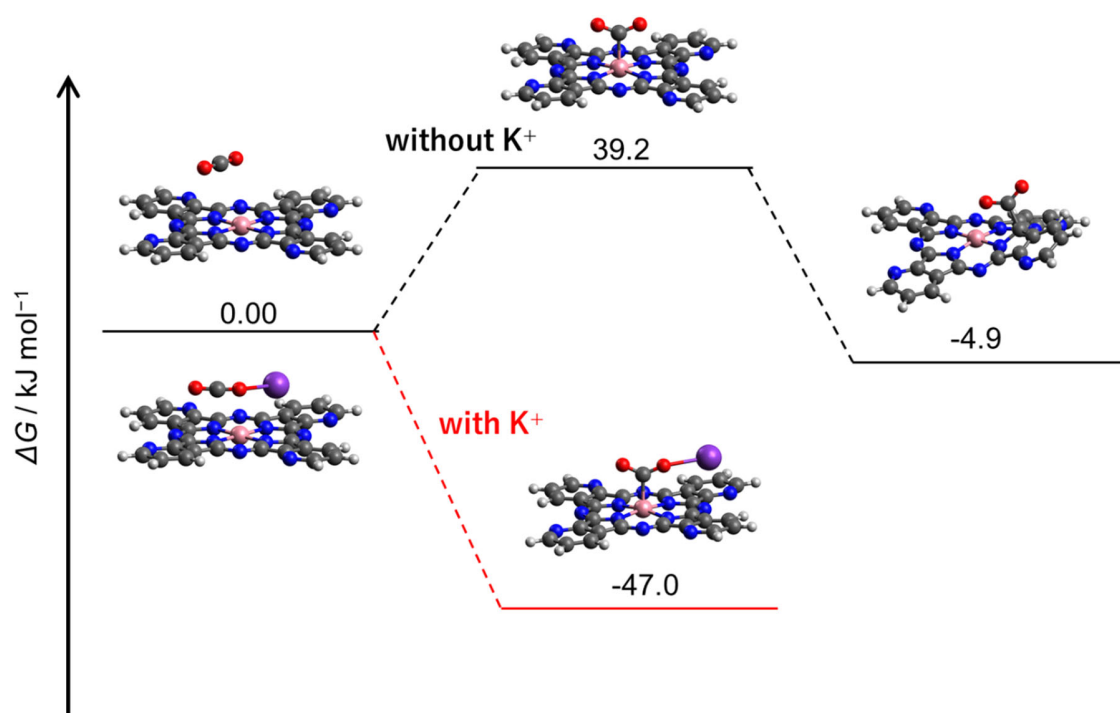
Figure S13 Results of DFT calculations of free energy changes during catalytic reaction steps involving the two-electron reduction species with $CO_2$ addition to the Co(PyPc) catalyst (elements color show White (Hydrogen), Black (Carbon), Blue (Nitrogen), Red (Oxygen), Purple (Potassium) and Pink (Cobalt)).



Figure S14 Results of DFT calculations of free energy changes during catalytic reaction steps involving the two-electron reduction species with $CO_2$ addition to the Co(Pc) catalyst (elements color show White (Hydrogen), Black (Carbon), Blue (Nitrogen), Red (Oxygen), Purple (Potassium) and Pink (Cobalt)).
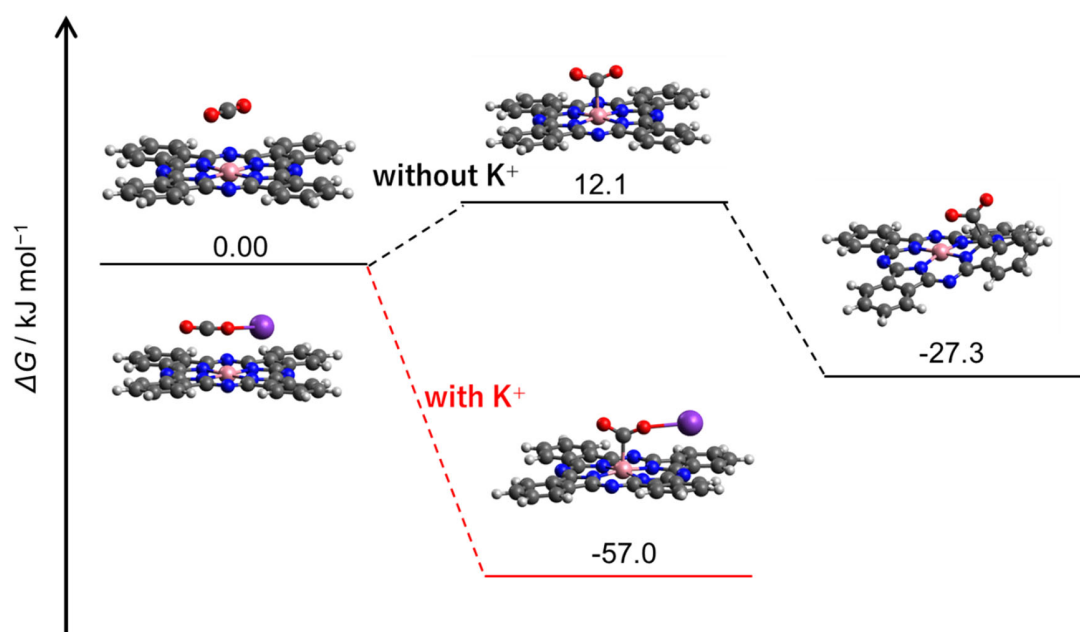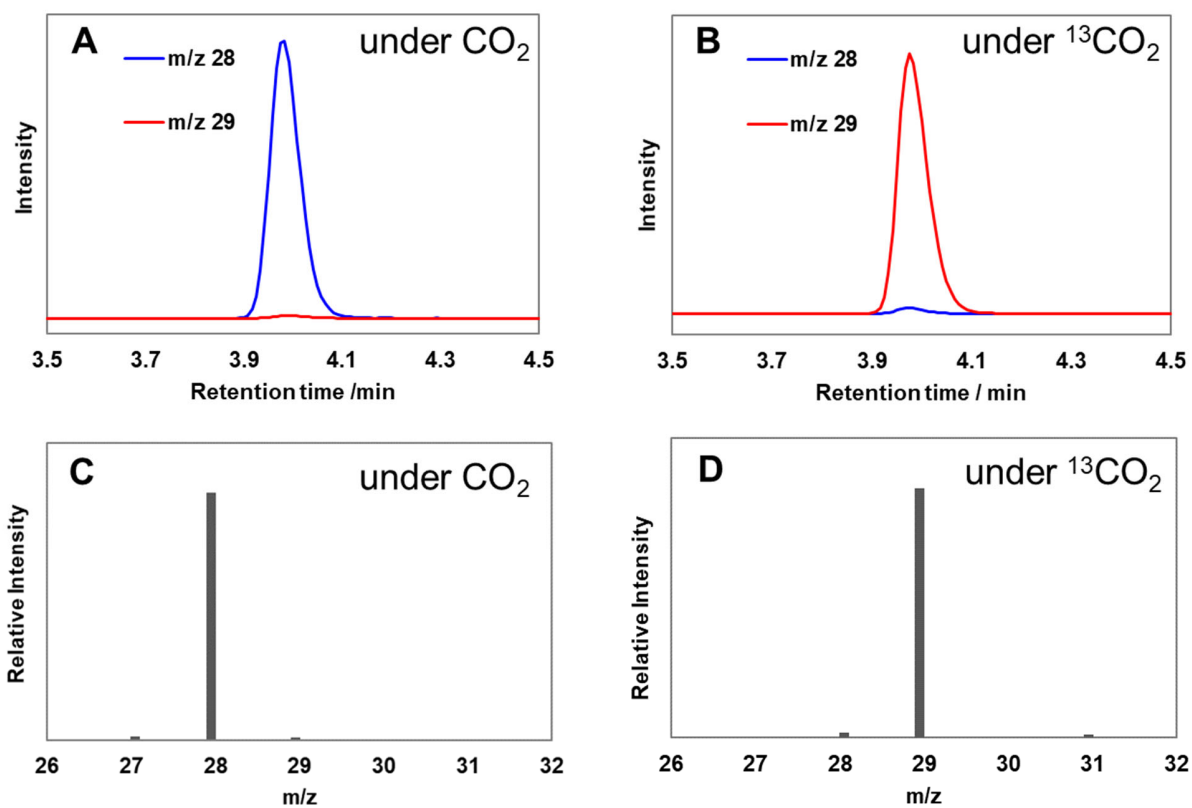
Figure S15. Data obtained during isotope tracer experiments involving electrochemical $CO_2$ reduction using the MEA cell with the Co(PyPc)+K/C cathode and Ni+Fe/Ni anode at -1.7 V with a flow of $CO_2$ or $^{13}CO_2$ for 20 min. GC-MS chromatograms acquired under (A) $CO_2$ and (B) $^{13}CO_2$, and mass spectra acquired at a retention time of 4 min under (C) $CO_2$ and (D) $^{13}CO_2$.
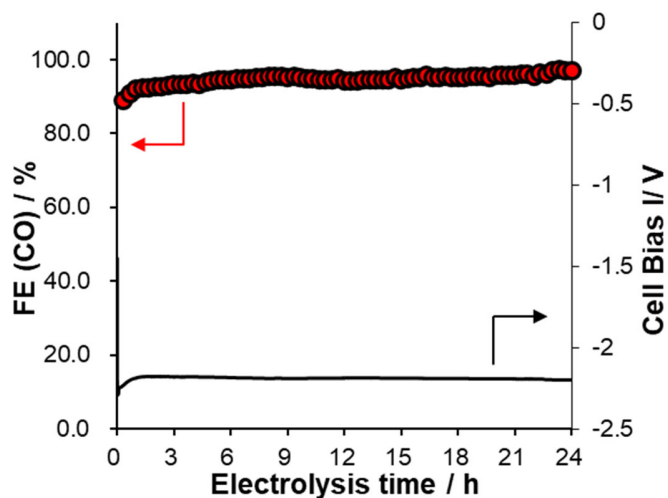
Figure S16. Electrocatalytic activity of the Co(PyPc)+K/C electrode loaded with 0.24 mg Co(PyPc) using the MEA cell during long-term bulk electrolysis at -50 mA/cm$^2$ as indicated by the Faradaic efficiency associated with CO production (FE(CO), red circles) and cell voltage at a constant current density of -50 mA/cm$^2$ (black line) using 0.2 M KHCO$_3$.
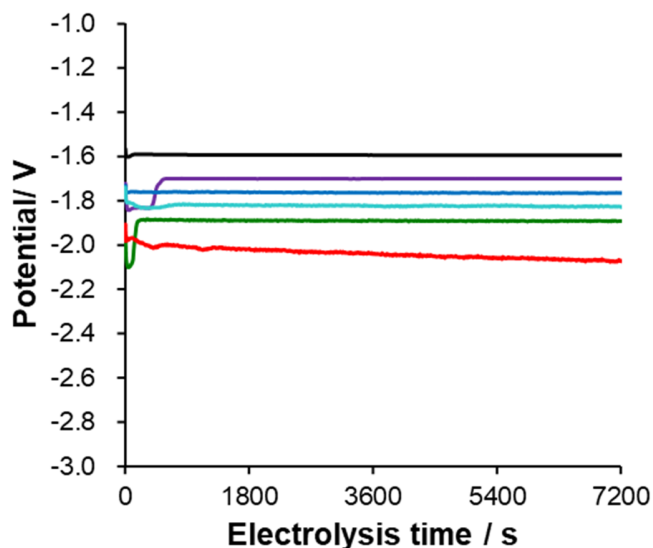


Figure S17. Chronopotentiometry data obtained during the reduction of CO$_2$ with 0.08 mg Co(PyPc)+K/C during 2 h of electrolysis using the MEA cell at several constant current densities [-10 mA/cm$^2$ (black), -25 mA/cm$^2$ (purple), -50 mA/cm$^2$ (blue), -75 mA/cm$^2$ (sky blue), -100 mA/cm$^2$ (green) and -150 mA/cm$^2$ (red)]. The resulting products are shown in Table 1.
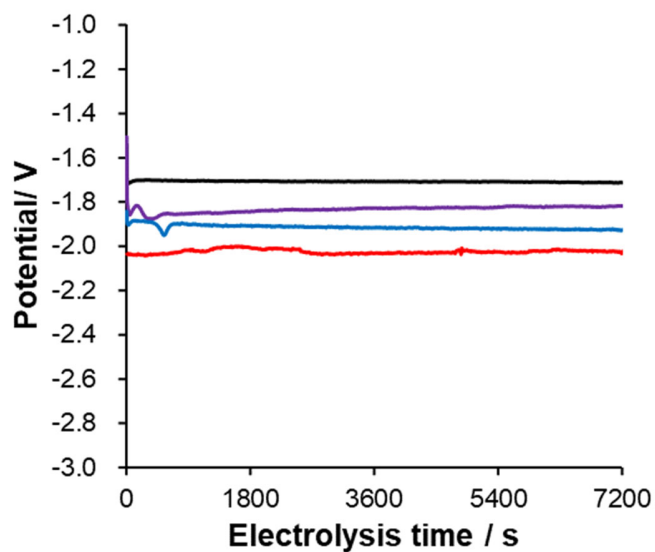
Figure S18. Chronopotentiometry data obtained employing a 0.24 mg/cm$^2$ Co(PyPc)+K/C electrode to catalyze CO$_2$ reduction over a 2 h time span using the MEA cell at several constant current densities [-50 mA/cm$^2$ (black), -100 mA/cm$^2$ (purple), -150 mA/cm$^2$ (blue) and -200 mA/cm$^2$ (red)]. The resulting products are summarized in Table 1.



Figure S19. Optimized molecular
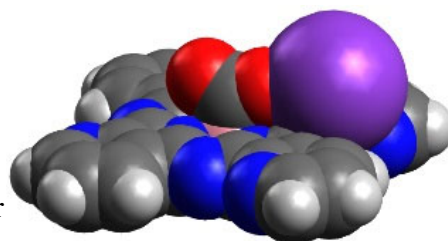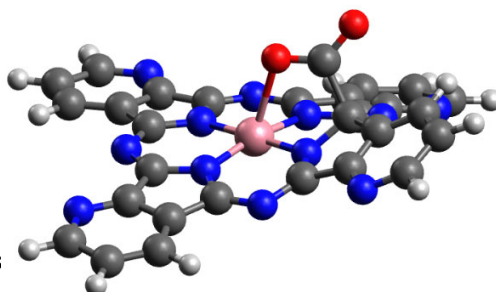


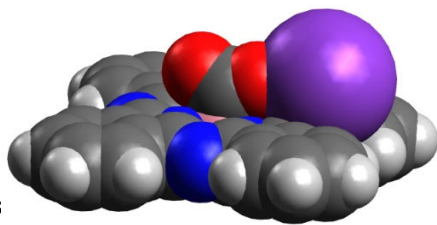Figure S20. Optimized molecul:

5



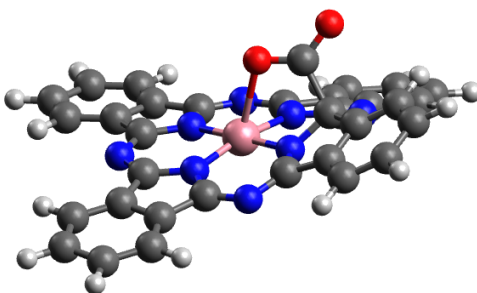Figure S21. Optimized molecula

10

15



Figure S22. Optimized molecula

**Table S1.** Summary of electrocatalytic $CO_2$ reduction using full-cell gas diffusion system.

| Cathode | Anode | Cell voltage / V | Current density / mA cm$^{-2}$ | Product (FE%) | Mass activity for CO /mA mg$^{-1}$ | Operation time / h | Reference |
|---|---|---|---|---|---|---|---|
| Co(PyPc)+K/C | Ni-Fe/Ni | -1.59 | 10 | CO (91 %) | 151.3 | 2 | this work |
| Co(PyPc)+K/C | Ni-Fe/Ni | -1.95 | 100 | CO (95 %) | 1636.7 | 168 | this work |
| Co(PyPc)*+K/C | Ni-Fe/Ni | -1.75 | 50 | CO (98 %) | 204.6 | 504 | this work |
| Co(PyPc)*+K/C | Ni-Fe/Ni | -2.03 | 200 | CO (95 %) | 793.3 | 2 | this work |
| Co(Pc)+K/C | NF | -2.1 | 100 | CO (94 %) | 522.2 | 24 | this work |
| Co(Pc)+phenol | NF | ca. -2.3 | 100 | CO (~98 %) | 24.5 | 3 | (19) |
| CoTMAPc@CNT | NF | ca. -1.9** | 31 | CO (94.5%) | 430.8 | 15 | (20) |
| CoPc-CN/CNT | CoOx/CNT | -2.0 | ca. 37.5 | CO (90%) | ca. 182 | 10 | (21) |
| CoPc/CNT-MD | IrTaOx/Ti | -3.0 | 50 | CO (90 to 80%) | ca. 5880 | 38 | (22) |
| NiPcP | NF | -2.6 | 80 | CO (no data) | - | 10 | (23) |
| Au | IrOx/Ti | -2.00 | 100.55 | CO (98.2%) | 548.8 | 8 | (24) |
| Au | IrOx/Ti | -2.25 | 185.84 | CO (85.0%) | 877.5 | 0.67 | (24) |
| Ag | IrOx | -3.0 | 50 | CO (95 %) | 47.5 | 4380 | (25) |
| Ag | IrOx | -2.75 | 100 | CO (95 %) | 190 | 30 | (26) |
| Ag | NiFeS@NF | -2.0 | 100 | CO (98.7 %) | 20 | 0.28 | (27) |
| Ag | NiFeDAT | -2.18 | 100 | CO (95 %) | 100 | 0.05 | (28) |
| Ag | IrOx | -2.5 | 230 | CO (101 %) | 115 | 0.067 | (29) |
| AgAu | IrOx | -3.7 | 202 | CO (93 %) | 101 | 70 | (30) |

* In these trials, 0.24 mg Co(PyPc) was loaded on the electrode. ** Electrode voltage with iR compensation. CNT = carbon nanotube, NF = Ni-foam

5

**Table S2.** Summary of electrocatalytic $CO_2$ reduction trials using Co complex catalysts with various additives in full-cell gas diffusion systems.

| Cathode catalyst | Anode catalyst | Additives | Cell voltage / V | Current density / mA cm$^{-2}$ | Product (FE%) | Operation time / h | Reference |
|---|---|---|---|---|---|---|---|
| Co(PyPc) | Ni-Fe/Ni | KOtf | -1.95 | 100 | CO (95 %) | 168 | this work |
| Co(PyPc) | Ni-Fe/Ni | KC$_4$F$_9$Otf | -1.90 | 100 | CO (95 %) | 24 | this work |
| Co(PyPc) | Ni-Fe/Ni | NaOtf | -1.86 | 50 | CO (93 %) | 24 | this work |
| Co(PyPc) | Ni-Fe/Ni | - | -2.07 | 100 | CO (~94 %) | 2 | this work |
| Co(Pc) | Ni-foam | KOtf | -2.1 | 100 | CO (94 %) | 24 | this work |
| Co(Pc) | Ni-foam | phenol | ca. -2.3 | 100 | CO (~98 %) | 3 | (*19*) |
| Co(Pc) | Ni-foam | - | ca. -2.7 | 100 | CO (~98 %) | 3 | (*19*) |

5

**Table S3.** Summary of electrocatalytic $CO_2$ reduction using full-cell gas diffusion system using carbonate salt solution.

| Cathode catalyst | Anode catalyst | Solvent | Cell voltage / V | Current density / mA cm$^{-2}$ | Product (FE%) | Operation time / h | Reference |
|---|---|---|---|---|---|---|---|
| Co(PyPc)+K | IrOx | 0.2M KHCO$_3$ | -2.2 | 50 | CO (94 %) | 24 | this work |
| CoPc/CNT-MD | IrTaOx/Ti | 0.5 M KHCO$_3$ | -3.0 | 50 | CO (90 to 80%) | 38 | (*22*) |
| Ag | IrOx | 0.01 M KHCO$_3$ | -3.0 | 50 | CO (95 %) | 4380 | (*25*) |
| AgAu | IrOx | 1M KHCO$_3$ | ~-4.0 | 100 | CO (80 %) | - | (*30*) |

10

**Table S4** Calculated Gibbs free energies ($G$) and $\Delta G_{ads}$ values for $CO_2$ adsorption reactions.

| reaction | Co(PyPc) | | | | Co(Pc) | | | |
|---|---|---|---|---|---|---|---|---|
| | $G$ (hartree) | | $\Delta G_{ads}$ | | $G$ (hartree) | | $\Delta G_{ads}$ | |
| | before adsorption | after adsorption | (hartree) | (kJ/mol) | before adsorption | after adsorption | (hartree) | (kJ/mol) |
| (1) | −2064.416504 | −2064.401577 | +0.014927 | +39.2 | −2000.241082 | −2000.236481 | +0.004601 | +12.11 |
| (2) | −2664.356214 | −2664.374088 | −0.017874 | −46.9 | −2600.177695 | −2600.200102 | −0.022407 | −58.8 |
| (3) | −2064.416504 | −2064.418383 | −0.001879 | −4.9 | −2000.241082 | −2000.251499 | +0.010417 | −27.3 |

5

## References

1. E. Villagra *et al.*, Tuning the redox properties of Co-N4 macrocyclic complexes for the catalytic electrooxidation of glucose. *Electrochimica Acta* **53**, 4883-4888 (2008).
2. T. M. Suzuki *et al.*, Highly Enhanced Electrochemical Water Oxidation Reaction over Hyperfine β-FeOOH(Cl):Ni Nanorod Electrode by Modification with Amorphous Ni(OH)2. *Bulletin of the Chemical Society of Japan* **91**, 778-786 (2018).
3. J. D. Chai, M. Head-Gordon, Long-range corrected hybrid density functionals with damped atom-atom dispersion corrections. *Physical Chemistry Chemical Physics* **10**, 6615-6620 (2008).
4. W. J. Stevens, M. Krauss, H. Basch, P. G. Jasien, RELATIVISTIC COMPACT EFFECTIVE POTENTIALS AND EFFICIENT, SHARED-EXPONENT BASIS-SETS FOR THE 3RD-ROW, 4TH-ROW, AND 5TH-ROW ATOMS. *Canadian Journal of Chemistry-Revue Canadienne De Chimie* **70**, 612-630 (1992).
5. V. A. Rassolov, M. A. Ratner, J. A. Pople, P. C. Redfern, L. A. Curtiss, 6-31G*basis set for third-row atoms. *Journal of Computational Chemistry* **22**, 976-984 (2001).
6. P. C. Hariharan, J. A. Pople, The influence of polarization functions on molecular orbital hydrogenation energies. *Theoretica chimica acta* **28**, 213-222 (1973).
7. W. J. Hehre, R. Ditchfield, J. A. Pople, Self—Consistent Molecular Orbital Methods. XII. Further Extensions of Gaussian—Type Basis Sets for Use in Molecular Orbital Studies of Organic Molecules. *The Journal of Chemical Physics* **56**, 2257-2261 (1972).
8. R. Ditchfield, W. J. Hehre, J. A. Pople, Self-Consistent Molecular-Orbital Methods. IX. An Extended Gaussian-Type Basis for Molecular-Orbital Studies of Organic Molecules. *The Journal of Chemical Physics* **54**, 724-728 (1971).
9. G. Scalmani, M. J. Frisch, Continuous surface charge polarizable continuum models of solvation. I. General formalism. *Journal of Chemical Physics* **132**, 114110 (2010).
10. J. Tomasi, B. Mennucci, R. Cammi, Quantum mechanical continuum solvation models. *Chemical Reviews* **105**, 2999-3093 (2005).
11. J. Tomasi, B. Mennucci, E. Cances, The IEF version of the PCM solvation method: an overview of a new method addressed to study molecular solutes at the QM ab initio level. *Journal of Molecular Structure-Theochem* **464**, 211-226 (1999).
12. B. Mennucci, J. Tomasi, Continuum solvation models: A new approach to the problem of solute's charge distribution and cavity boundaries. *Journal of Chemical Physics* **106**, 5151-5158 (1997).
13. B. Mennucci, E. Cances, J. Tomasi, Evaluation of solvent effects in isotropic and anisotropic dielectrics and in ionic solutions with a unified integral equation method: Theoretical bases, computational implementation, and numerical applications. *Journal of Physical Chemistry B* **101**, 10506-10517 (1997).
14. E. Cances, B. Mennucci, J. Tomasi, A new integral equation formalism for the polarizable continuum model: Theoretical background and applications to isotropic and anisotropic dielectrics. *Journal of Chemical Physics* **107**, 3032-3041 (1997).
15. M. J. Frisch *et al.* (Wallingford, CT, 2016).
16. R. Shannon, Revised effective ionic radii and systematic studies of interatomic distances in halides and chalcogenides. *Acta Crystallographica Section A* **32**, 751-767 (1976).
17. S. Sato, K. Saita, K. Sekizawa, S. Maeda, T. Morikawa, Low-Energy Electrocatalytic CO2 Reduction in Water over Mn-Complex Catalyst Electrode Aided by a Nanocarbon Support and K+ Cations. *ACS Catalysis* **8**, 4452-4458 (2018).

18.   T. Nonaka *et al.*, Quick-scanning x-ray absorption spectroscopy system with a servo-motor-driven channel-cut monochromator with a temporal resolution of 10 ms. *Review of Scientific Instruments* **83**, 083112 (2012).

19.   S. Ren *et al.*, Molecular electrocatalysts can mediate fast, selective CO2 reduction in a flow cell. *Science* **365**, 367-369 (2019).

20.   J. Su *et al.*, Building a stable cationic molecule/electrode interface for highly efficient and durable CO2 reduction at an industrially relevant current. *Energy & Environmental Science* **14**, 483-492 (2021).

21.   X. Lu *et al.*, High-Performance Electrochemical CO2 Reduction Cells Based on Non-noble Metal Catalysts. *Acs Energy Letters* **3**, 2527-2532 (2018).

22.   X. Wu *et al.*, Molecularly Dispersed Cobalt Phthalocyanine Mediates Selective and Durable CO2 Reduction in a Membrane Flow Cell. *Advanced Functional Materials* **32**, 2107301 (2021).

23.   S. Wei *et al.*, Conjugated nickel phthalocyanine polymer selectively catalyzes CO2-to-CO conversion in a wide operating potential window. *Applied Catalysis B: Environmental* **284**,   119739 (2021).

24.   S. Verma *et al.*, Insights into the Low Overpotential Electroreduction of CO2 to CO on a Supported Gold Catalyst in an Alkaline Flow Electrolyzer. *Acs Energy Letters* **3**, 193-198 (2018).

25.   R. B. Kutz *et al.*, Sustainion Imidazolium-Functionalized Polymers for Carbon Dioxide Electrolysis. *Energy Technology* **5**, 929-936 (2017).

26.   W. H. Lee *et al.*, Highly selective and scalable CO2 to CO - Electrolysis using coral-nanostructured Ag catalysts in zero-gap configuration. *Nano Energy* **76**, 105030 (2020).

27.   S. Li *et al.*, Polymer-Supported Liquid Layer Electrolyzer Enabled Electrochemical CO2 Reduction to CO with High Energy Efficiency. *ChemistryOpen* **10**, 639-644 (2021).

28.   S. S. Bhargava *et al.*, Decreasing the Energy Consumption of the CO2 Electrolysis Process Using a Magnetic Field. *ACS Energy Letters* **6**, 2427-2433 (2021).

29.   S. Verma, X. Lu, S. C. Ma, R. I. Masel, P. J. A. Kenis, The effect of electrolyte composition on the electroreduction of CO2 to CO on Ag based gas diffusion electrodes. *Physical Chemistry Chemical Physics* **18**, 7075-7084 (2016).

30.   J. Li *et al.*, Metal Oxide Clusters on Nitrogen-Doped Carbon are Highly Selective for CO2 Electroreduction to CO. *ACS Catalysis* **11**, 10028-10042 (2021).